Influence of the Atlantic Meridional Overturning Circulation on the Tropical Climate Response to CO2 Forcing

Jessica Vial, Christophe Cassou, Francis Codron, Sandrine Bony, Yohan Ruprich-Robert

Influence of the Atlantic meridional overturning circulation on the tropical climate response to CO_2 forcing

Jessica Vial[1,2], Christophe Cassou[3], Francis Codron[1], Sandrine Bony[4] and Yohan Ruprich-Robert[5]

[1]LOCEAN/IPSL, Sorbonne Université, CNRS, Université Pierre et Marie Curie, France
[2]Max Planck Institute for Meteorology, Hamburg, Germany
[3]Université de Toulouse, CECI, CNRS-Cerfacs, France
[4]LMD/IPSL, Sorbonne Université, CNRS, Université Pierre et Marie Curie, France
[5]Barcelona Supercomputing Center, Barcelona, Spain

Key Points:

- Internal multidecadal variability is an important modulator of the tropical climate response to CO_2 forcing
- By impacting global atmospheric energetics, AMOC fluctuations affect the strength of the mean atmospheric tropical circulation
- The dependence of the CO_2-forced circulation response to AMOC-related background state follows a "strong-gets-weaker" pattern

Corresponding author: Jessica Vial, jessica.vial@mpimet.mpg.de

Abstract

The increase of atmospheric greenhouse gases is expected to affect the hydrological cycle and large-scale precipitation patterns. In parallel, unforced natural variability on decadal to multidecadal timescales can also modulate forced changes at the regional scales. Based on multi-member ensembles from a coupled General Circulation Model, we investigate the sensitivity of CO_2-forced changes in tropical precipitation and atmospheric circulation to fluctuations of the Atlantic Multidecadal Overturning Circulation (AMOC). We show that contrasted AMOC states yield considerable differences in equatorial Pacific precipitation forced changes, by impacting the direct (within a year) CO_2-induced weakening of the Walker circulation. We use global atmospheric energetics, as a theoretical backdrop, to explain the relationship between the tropical atmospheric circulation and the AMOC state. A physical mechanism is then proposed, relating the direct CO_2-forced weakening of the atmospheric tropical circulation to its climatological strength in unperturbed climate, and indirectly to the AMOC state.

1 Introduction

Predicting the precipitation response to increasing greenhouse gases (GHG) atmospheric concentration remains a great scientific challenge. The need to better anticipate future precipitation changes is particularly strong in the tropics where nearly 50% of the Earth's population is influenced by rainfall and monsoon variability [*De Carvalho*, 2016]. Past investigations have led to considerable progress in our understanding of the key factors controlling the long-term (centuries ahead) precipitation forced-response assessed from coupled models under specific GHG emission scenarios [*Chou and Neelin*, 2004; *Held and Soden*, 2006; *Chou et al.*, 2009; *Seager et al.*, 2010; *Xie et al.*, 2010; *Bony et al.*, 2013; *Chadwick et al.*, 2013]. Physical mechanisms have also been proposed to explain the considerable spread among the models' projections [*Ma and Xie*, 2013; *Xie et al.*, 2015; *Long et al.*, 2016; *Oueslati et al.*, 2016]. On the other hand, few studies so far have evaluated the importance of the decadal-to-multidecadal internal variability in modulating the long-term response of regional rainfall to anthropogenic forcing [*Xie et al.*, 2015; *Cassou et al.*, 2018], despite the dominant contribution of natural climate variability to uncertainties in regional precipitation projections [*Hawkins and Sutton*, 2011].

This study aims at exploring and understanding the weight/fingerprint of the multidecadal internal variability in the estimation of GHG-forced precipitation changes in the tropics using the CNRM-CM5 atmosphere-ocean coupled model. Abrupt doubling CO_2 experiments have been carried out to extract the forced response. Multi-member ensembles are built here to evaluate the sensitivity (or interaction) of the forced response to (with) the variability of the Atlantic Meridional Overturning Circulation (AMOC). In CNRM-CM5, AMOC fluctuations are associated with surface ocean fin-

gerprint, which projects on the so-called Atlantic Multidecadal Variability (AMV) pattern. In this model, the AMV corresponds to the leading mode of surface temperature internal low-frequency variability at global scale. Spectral analysis shows maximum energy concentration within the 80-120yr band as assessed from the long 850-yr preindustrial control (piControl) experiment [*Ruprich-Robert and Cassou*, 2015] produced for the fifth phase of the Coupled Model Intercomparison Project (CMIP5, [*Taylor et al.*, 2012]).

In the following, abrupt CO_2-doubling experiments are initialized from two extreme phases of the model AMOC and the impact of the initial ocean state on the tropical precipitation forced-response is analyzed by contrasting the two distinct ensembles. Each of them includes 10 members differing by their first day atmospheric states so that the full range of uncertainties associated with internal variability (ocean + atmosphere) is covered – because of the combination of both macro and micro perturbations for the ensemble generation, following *Hawkins et al.* [2016] terminology. This protocol contrasts to most previous studies, which either combine single model realization from several models [*Vecchi and Soden*, 2007; *Long et al.*, 2016; *Oueslati et al.*, 2016] or which assess uncertainties through the sole atmospheric state sensitivity [*Selten et al.*, 2004; *Deser et al.*, 2012; *Kang et al.*, 2013].

The rationale for the choice of selecting two contrasted states of AMOC internal variability from a given model relies on the fact that observational records over the historical period (on which anthropogenic forcing is active) are too short to know the actual stage of AMOC with respect to its own long-term variability. This is an irreducible source of uncertainties for the forced response, which should be quantified and better understood.

The rest of the paper is outlined as follows. The model simulations and methodology are described in Section 2. Following an overview of the AMOC fingerprints in the CNRM-CM5 Model (Section 3), we analyze the sensitivity of the projected changes in tropical precipitation and circulation to the strength of the AMOC (Section 4), and propose a physical interpretation (Section 5). Conclusions and discussion are given in Section 6.

2 Materials and method

2.1 Climate model simulations

We use the CNRM-CM5.1 Coupled General Circulation Model developed for CMIP5. The atmospheric component is the spectral ARPEGE-Climat-5.2 model, with a Gaussian grid of $\sim$1.4° horizontal resolution and a vertical discretization over 31 levels (including 26 levels in the troposphere). The ocean model is NEMO (Nucleus for European Modeling of the Ocean) on the grid of $\sim$1° horizontal resolution and a vertical discretization over 42 levels (including 18 levels in the upper 250-m mixed layer ocean). See *Voldoire et al.* [2013] for a complete description of the model.

Oceanic conditions of Jan 1^{st} of year 303 and 141 are selected from the 850-year piControl experiment of CNRM-CM5 for the production of two unforced ensembles of 30 years and 10 members each. These two dates cor-

respond to extreme opposite states of the AMOC in piControl (-4.1 and +2.8 standard deviation, respectively) associated with very pronounced negative and positive phases of AMV, respectively [see Fig. 4 in *Ruprich-Robert and Cassou*, 2015]. Individual members of each ensemble (hereafter referred to as Pcold and Pwarm) differ only by their atmospheric initial conditions, chosen randomly [see *Ménégoz et al.*, 2017, for a complete description of the protocol]. Two twin ensemble experiments (i.e., identical initial conditions) are conducted (hereafter referred to as Fcold and Fwarm) with an instantaneous doubling of atmospheric CO_2 (abrupt2xCO2 relative to preindustrial conditions using CMIP5 nomenclature) imposed at the beginning of the simulations and then hold fixed.

2.2 Calculations and notations

Here are the calculations and notations of the different metrics applied on annually-averaged fields from the ensembles:

- ΔX is the projected climate response to CO_2 abrupt doubling for a given ensemble ($X_F - X_P$). When applicable, we evaluate both the 30-year averaged change and the contribution arising from the 1^{st}-year only [as an approximation of the direct CO_2-forced fast response, *Bony et al.*, 2013].
- δX stands for the anomaly of a given member with respect to the two-ensemble mean. ∂X is the anomaly expressed in percentage, or fractional difference (relative to the two-ensemble mean).
- The statistical significance of AMOC-related ensemble mean differences (based upon $p < 0.10$, unless otherwise stated) is evaluated against a null hypothesis of zero change using a 2-sided Student's t-test.

- I refers to as the tropical atmospheric overturning circulation index defined by *Bony et al.* [2013]. $I \equiv \omega_{500} \downarrow -\omega_{500} \uparrow$ with upward ($\omega_{500} \uparrow < 0$) and downward ($\omega_{500} \downarrow > 0$) pressure vertical velocities at 500 hPa averaged over 35°S-35°N.
- H is the Hadley circulation index defined as I, but on zonally averaged values of ω_{500} over 35°S-35°N.
- W is the Pacific Walker circulation index defined as the difference between $\omega_{500} \uparrow$ over the western/central Pacific (15°S-15°N, 110°E-160°W) and $\omega_{500} \downarrow$ over the eastern basin (15°S-15°N, 80°-140°W). When applicable, we compute W over land + ocean or just ocean areas.

- The top of the atmosphere (TOA) instantaneous radiative forcing (RF) quantifies the direct radiative impact of the doubling CO_2 concentration alone. It is commonly diagnosed from offline radiative transfer simulations [e.g., *Collins et al.*, 2006], but due to the large number of ensemble experiments considered, we use the simple linear (least squares) regression model developed by *Huang et al.* [2016]: $RF =$

$\overline{RF} + \sum_i A_i \frac{y_i - \overline{y_i}}{\overline{y_i}}$, where A_i is the regression coefficient of a dependent variable y_i with global mean multiyear mean $\overline{y_i}$, and $\overline{RF}$, the intercept of the regression model, represents the global mean of RF. This regression model accounts for several dependent variables i, which are taken from the P-ensemble simulations, including the temperature at the surface and at 10 hPa, the vertically-integrated water vapor and the cloud radiative forcing (difference between all-sky and clear-sky radiation fluxes at the TOA). See *Huang et al.* [2016] for more details.

- R_a refers to the column-integrated atmospheric radiative fluxes ($R_a = R_{TOA} - R_{surface}$, positive fluxes upward). The 1^{st}-year change in R_a is used as an approximation of the direct CO_2-forced radiative heating in the atmosphere.
- $\delta_x RF$ and $\delta_x R_a$ are zonal gradients of RF and R_a over the equatorial Pacific estimated by the difference between (15°S-15°N, 110°E-160°W) and (15°S-15°N, 80°-140°W), as in W calculation.

3 AMOC fingerprints in CNRM-CM5

Figure 1 illustrates the yearly evolution of AMOC and Global Mean Surface Temperature (GMST) for the two 10-member P and F ensembles over the 30 years of integration. The model exhibits significant and persistent initial value predictability for both quantities as expected from spectral properties and physical mechanisms of AMOC variability assessed from piControl [*Ruprich-Robert and Cassou*, 2015]. The 10-member Pcold and Pwarm ensembles for the AMOC time-series are clearly disjoint throughout the entire 30 years of simulations (Fig. 1a). This is a fortiori true for AMOC ensemble means, as well as for GMST, with a difference of ∼2.5 Sv and 0.11°C, respectively.

Regionally, the AMOC fingerprints in CNRM-CM5 are consistent with previous inferences from observations and model-based studies [see *Buckley and Marshall*, 2016, for a review]. Difference between Pcold and Pwarm ensembles show a significant (marginal) surface and tropospheric cooling (warming) over the northern (southern) hemisphere when AMOC is weak due to reduced northward ocean heat transport. A southward displacement of the Hadley circulation and ITCZ-related precipitation from their climatological position is obtained consistently with the modification of the mean inter-hemispheric gradient (Supplementary Fig. 1 and *Ménégoz et al.* [2017] for further description). A contraction and reinforcement of the Walker cell branches in the Pacific is also noticeable. Therefore, the AMOC-related anomalies are planetary and persistent so that the two ensembles can be treated as samples for two contrasted mean background states set by pure internal variability.

AMOC declines steadily in response to abrupt CO_2 forcing, but the two ensembles clearly remain disjoint over the 30-yr integration (Fig. 1c). Rapid warming occurs in both F-ensembles, which stay statistically distinguishable in GMST up to ∼15 years (Fig. 1d). These emphasize on the

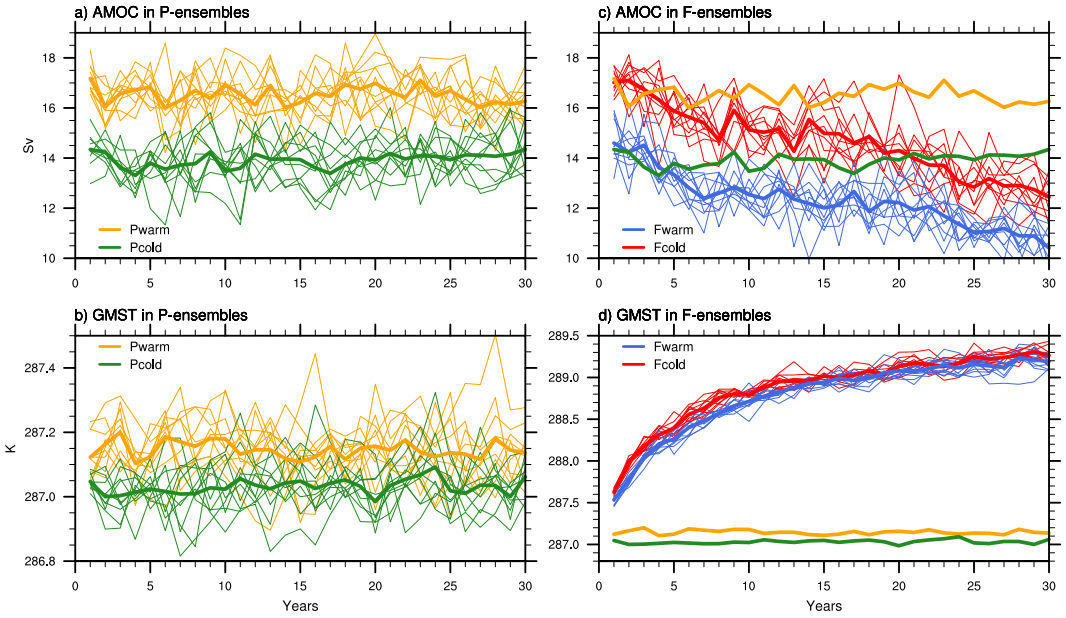

Figure 1: Yearly evolution of (a) AMOC and (b) GMST for Pwarm (orange) and Pcold (green) ensembles. Thin lines stand for individual members and thick lines for ensemble means. (c, d) same but for Fwarm (red) and Fcold (blue) ensembles, with the P-ensemble mean quantities reproduced for reference.

very strong persistence properties of AMOC in the model despite extreme forcing perturbation.

4 Sensitivity of precipitation and circulation forced-responses to AMOC states

The tropical precipitation and tropospheric circulation responses to CO_2 forcing and their modulation by different AMOC-related background states are presented in Figure 2. The CNRM-CM5 model exhibits increased rainfall in most of the deep tropics and enhanced drying over subtropical regions, similar to previous CMIP3/CMIP5 assessments [e.g., *Seager et al.*, 2010; *Xie et al.*, 2015; *Long et al.*, 2016; *Oueslati et al.*, 2016]. Focus is laid on the tropical Pacific region, as it is where the fingerprint of multi-decadal internal variability in the forced responses is the most important. Differences in rainfall changes between the cold and warm AMOC-related states are in the same order of magnitude (Fig. 2c) as the individual CO_2-induced response assessed from ensemble-mean changes (Fig. 2a, b). This clearly indicates that AMOC is an important modulator of the projected forced-changes in this region. Comparison of Figures 2c and 2f shows that the impact of different AMOC states on precipitation forced-responses is strongly related to circulation changes (pattern correlation equals to 0.95). A stepwise analysis of the vertically-integrated water budget equation further demonstrates that the mean circulation changes alone can provide a full accounting of the difference in the equatorial Pacific rainfall changes between the cold and warm ensembles (Supplementary Fig. 2 to 4). More-

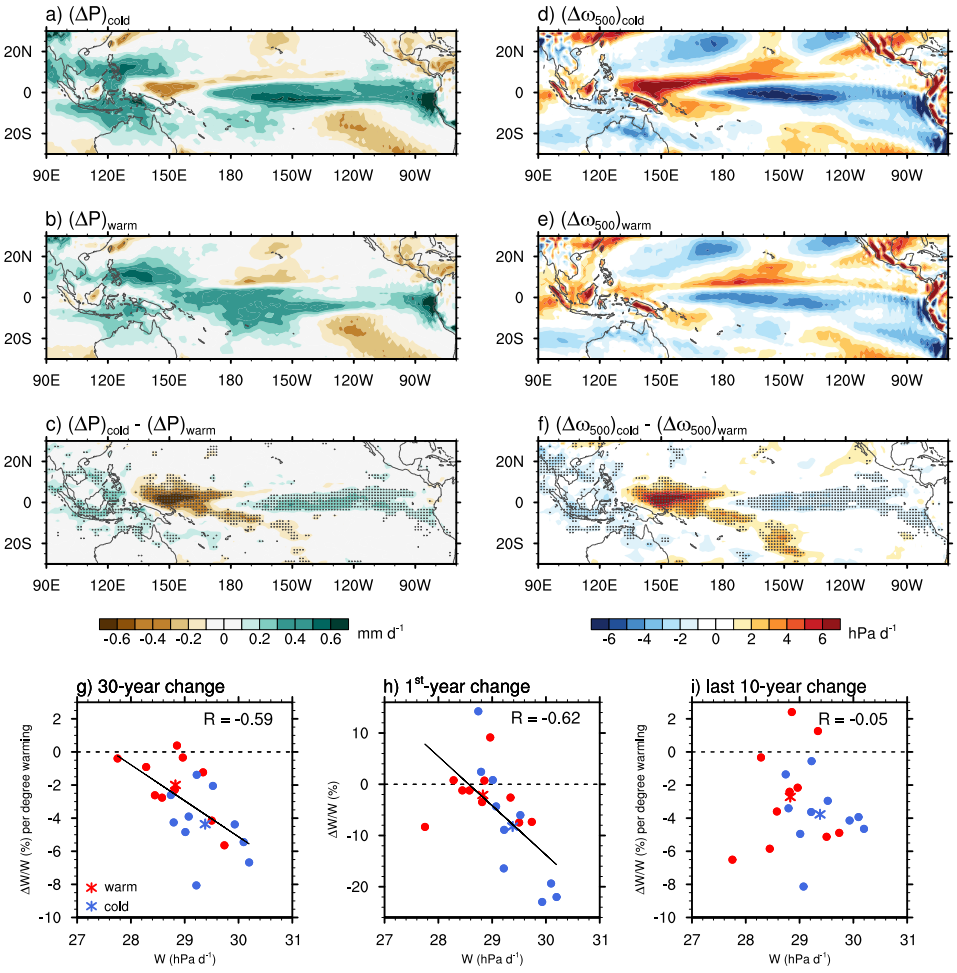

Figure 2: (a – c) 30-year mean response to CO_2 forcing in precipitation for (a) cold and (b) warm ensemble means over tropical Pacific (30°S-30°N, 90°E-70°W) and (c) AMOC-related difference between cold and warm ensembles (hatching indicating statistical significance). (d – f) same but for pressure vertical velocity at 500 hPa. (g – i) fractional forced changes (relative to P-ensembles) in Walker circulation as a function of its mean intensity in P-ensembles for warm (red) and cold (blue) ensembles: (g) 30-year mean change per degree of global surface warming, (h) 1^{st}-year change and (i) last 10-year mean change per degree of global surface warming. Each individual member is represented by a filled circle and the ensemble means by asterisks.

over, a decomposition of Figure 2f into its zonally averaged and zonally asymmetric component suggests that most of the modulation in rainfall changes originates from differences in the Walker circulation changes rather than in the Hadley circulation changes (Supplementary Fig. 5). The overall weakening of the Walker circulation (defined in Section 2.2) is amplified by a factor of two in the cold ensemble (Fig. 2g). This occurs almost everywhere across equatorial Pacific, but more particularly over the ocean (Fig. 2d – f). We further show that the direct CO_2-forced Walker circulation response (Fig. 2h), rather than the temperature-mediated transient circulation response (Fig. 2i), explains to a large extent the sensitivity of precipi-

tation forced-changes to AMOC states. Figure 2h shows a significant initial value predictability of the direct CO_2-forced Walker circulation responses. The large range of projected changes in Walker circulation depends on its climatological strength: the Walker circulation is more strongly reduced when it is stronger a priori in the preindustrial control climate state (Fig. 2h). This relationship is even stronger when W is computed over ocean areas only (correlation R $= 0.7$ – not shown).

In the next section, we investigate the physical mechanism controlling these contrasted circulation responses to CO_2 forcing. To this end, we address two questions: (i) How do different AMOC-related states influence the tropical mean circulation in the control climate state? (Section 5.1); (ii) Why does the direct circulation response to increased CO_2 depend on the mean background state? (Section 5.2).

5 Physical understanding

5.1 AMOC-related influence on tropical circulation in control climate

Global constraints on precipitation and water vapor are commonly used to understand the tropical circulation response to global warming [e.g., *Mitchell et al.*, 1987; *Held and Soden*, 2006; *Vecchi and Soden*, 2007]. We here apply the same energetic constraints to explain the sensitivity of the tropical mean overturning circulation to the AMOC state, since the latter has a global influence on the modeled climate (Fig. 1b and Supplementary Fig. 1) and thus justifies the use of such a conceptual framework.

When the AMOC is weaker in control experiments, the surface temperature decreases significantly by 0.11K (globally) and by 0.04K (in the tropics). As shown in Figure 3, this decrease in temperature is also associated with (i) a decrease in precipitation of 1.6%/K (Fig. 3a) that results from a weaker radiative cooling and surface evaporation (not shown) and (ii) a decrease in column water vapor amount following the Clausius-Clapeyron constraint of 7%/K (Fig. 3b). Following *Mitchell et al.* [1987], this differential response of the tropical (or equivalently global) mean decrease in precipitation and humidity to surface cooling can be used to estimate the fractional increase of the tropical overturning circulation in response to surface cooling. Using $\delta M/M = \delta P/P - 0.07\delta T_s/T_s$ [*Held and Soden*, 2006; *Vecchi and Soden*, 2007], where M is the convective mass flux, P is the precipitation and T_s the surface temperature, we expect an overall strengthening of the convective mass fluxes by 5.4%/K in the cold ensemble (Fig. 3c). The relationship between this theoretical strengthening in convective mass flux and the actual change in the overturning circulation simulated by the model is fairly good with ensemble means lying right on top of the expected line set by the theory (Fig. 3d). This confirms that the influence of AMOC on the tropical mean circulation corresponding to pure by-products of internal climate processes can be very well explained by the latter conceptual framework.

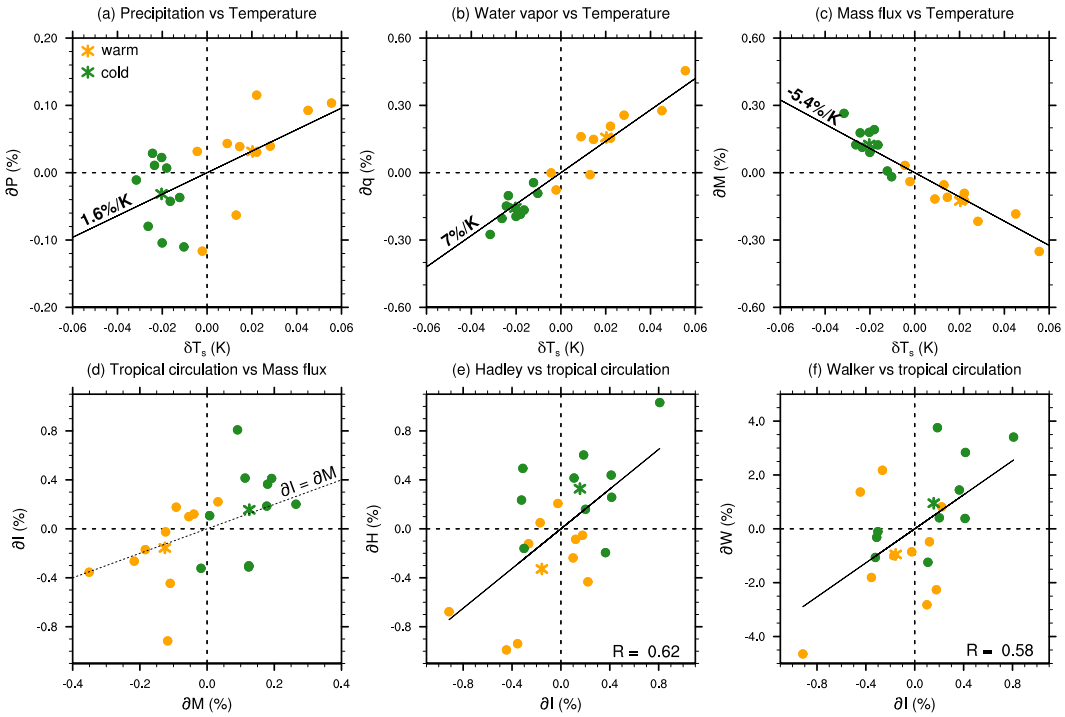

Figure 3: (a – c) AMOC-related fractional differences (∂X in Section 2.2) for tropically-averaged (a) precipitation, (b) vertically-integrated water vapor and (c) convective mass flux – estimated as the difference between (a) and (b) as in *Vecchi and Soden* [2007] – as a function of AMOC-related absolute differences in tropically-averaged surface temperature (δT_s, in K). (d – e) AMOC-related fractional differences for the tropically-averaged (d) overturning circulation, (e) Hadley circulation and (f) Walker circulation as a function of AMOC-related fractional differences in the estimated tropical convective mass flux (in d) and in the simulated overturning circulation (in e, f). All differences are significant at p<0.03. The color code is the same as Figure 1 for P-ensembles; warm (orange) and cold (green) members are shown by filled circles and their respective ensemble means by asterisks. Also reported in (a – c) is the slope of the least-square regression fits (solid lines). In (d) the dashed line highlights the one-to-one relationship between ∂I and ∂M.

The AMOC-related change in the tropical overturning circulation is also reflected in the Hadley and Walker circulations, which are significantly reinforced when AMOC is weaker (Fig. 3e, f). Note that other factors control the Hadley and Walker circulations, influencing the exact magnitude of their AMOC-forced intensification and their relationships to the tropical mean overturning circulation. These factors could result from a redistribution of the convective and subsiding areas, which often accompanies the change in the intensity of the tropical overturning circulation [e.g., *Vecchi and Soden*, 2007] or in the northward ocean heat transport [e.g., *L'hévéder et al.*, 2015]. When AMOC is weak, the overall strengthening of the Walker and Hadley circulations is here associated with an eastward shift of convection over the central equatorial Pacific (Supplementary Fig. 1d) and a southward shift of the Hadley circulation, resulting in a strengthening (weakening) of the northern (southern) cell (Supplementary Fig. 1e). De-

spite this phenomenon, our analysis suggests that the global constraints on precipitation and water vapor are not only useful to understand the mean circulation weakening with global surface warming, but also the relationship between the multidecadal variations of the global mean surface temperature and of the tropical overturning circulation (Hadley/Walker) associated with the AMOC internally generated fluctuations. These results are robust across a large ensemble of CMIP5 models, except maybe for the AMOC-related variations in the Hadley circulation, which appear more model-dependent (Supplementary Text 2 and Fig. 6).

5.2 Dependence of the direct CO_2-forced response on the background state

We now explore the reasons why the direct effect of CO_2 on the Walker circulation depends on the climatological strength of the Walker circulation in the preindustrial climate state, and thus on the state of the AMOC (cf. Fig. 2h). One mechanism, proposed by *Merlis* [2015], relates the direct weakening of the overturning circulation to the spatial structure of the instantaneous radiative forcing to increased CO_2. The argument is based on the moist energetics of the tropical atmosphere, which constrain the mean overturning circulation to export energy from energy-rich (warm/moist) regions toward relatively energy-poor (cold/dry) regions [*Neelin and Held*, 1987; *Trenberth and Stepaniak*, 2004].

As shown by *Huang et al.* [2016], the spatial structure of the instantaneous radiative forcing strongly depends on the horizontal gradients of atmospheric and surface variables of the control climate state, especially surface and atmospheric temperature, atmospheric humidity and clouds. Figure 4a shows that the CO_2 radiative forcing (as estimated by *Huang et al.* [2016] - see also Section 2.2) is stronger in large-scale subsidence areas and weaker in regions of large-scale rising motions (compare RF with black contours in Fig. 4a). This dependence of the forcing on the mean circulation is explained by the presence of deep convective clouds and strong water vapor mixing ratios in regions of large-scale ascent, which masks the effect of increased CO_2 on TOA radiative fluxes [*Merlis*, 2015; *Huang et al.*, 2016, 2017; *Xia and Huang*, 2017]. [*Trenberth and Stepaniak*, 2004]. Over the tropical oceans, much of the instantaneous radiative forcing is confined to the atmosphere [e.g., *Huang et al.*, 2017; *Xia and Huang*, 2017]. Therefore, the effect of the spatially inhomogeneous radiative forcing, shown in Fig. 4a, is to radiatively heat the atmosphere more strongly in the subsiding than ascending region (as suggested in Fig. 4b by the 1^{st}-year change in R_a), which then requires the circulation to weaken to restore local atmospheric energetics. This also suggests that when the tropical overturning circulation is stronger in the control climate state, cloud and water vapor gradients between convective and subsidence areas are reinforced, and the larger spatial heterogeneity of the CO_2 forcing potentially leads to a stronger weakening of the circulation.

Consistent with this interpretation and because the Walker circulation is stronger when the AMOC is weaker (in the cold ensemble), the TOA ra-

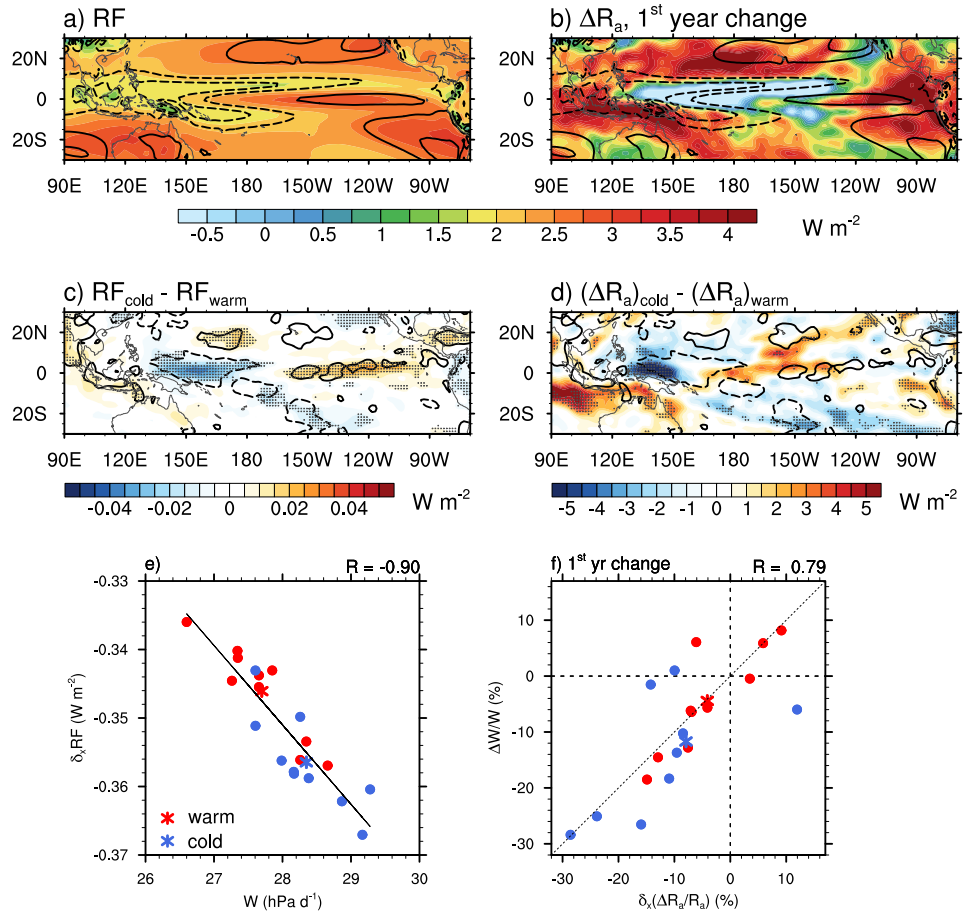

Figure 4: (a – b) The two-ensemble mean (a) instantaneous CO_2 radiative forcing (RF in Section 2.2, shaded) and (b) 1^{st}-year change in atmospheric radiative cooling (ΔR_a in Section 2.2, shaded); overlayed contours represent the two-ensemble mean 30-year mean atmospheric circulation (ω_{500}) for the P-ensembles. (c – d) AMOC-related difference for (c) RF and (d) ΔR_a; hatching indicating statistical significance and overlayed contours show the AMOC-related difference in ω_{500}. (e) Zonal gradient in RF ($\partial_x RF$ in Section 2.2) as a function of Walker circulation in the P-ensembles. (f) 1^{st}-year fractional change (compared with P-ensembles) in Walker circulation as a function of $\partial_x RF$. W is computed over ocean areas only to ensure that the relationships are not influenced by land-sea contrasts. The legend is similar to Figure 2: warm (red) and cold (blue) members are shown by filled circles and their respective ensemble means by asterisks.

diative forcing and 1^{st}-year atmospheric radiative heating are found to be (i) stronger in the eastern equatorial Pacific, where the subsiding branch of circulation is stronger, and (ii) weaker in the central equatorial Pacific region, where the rising branch of circulation is stronger (Fig. 4 c,d and 4 e). Therefore, the stronger Pacific equatorial zonal gradient in radiative forcing that is produced in the cold ensemble is expected to induce a stronger weakening of the Walker circulation by the direct effect of CO_2 on the atmospheric radiative fluxes (as suggested in Figure 4 f).

6 Conclusion

In this study, the tropical precipitation and tropospheric circulation responses to CO_2 forcing and its modulation by different states of the Atlantic Multidecadal Overturning Circulation (AMOC) have been investigated using multi-member ensembles from the fully coupled CNRM-CM5 General Circulation Model. A very large range of possible precipitation projections is obtained in the equatorial Pacific region due to pure internal variability, assessed here through an ensemblist approach and a combination of macro and micro perturbations for its generation. The associated uncertainties are comparable to – or even larger than – the forced response estimated through ensemble-mean changes. This underscores the crucial need for realizing multi-member ensembles (by sampling both atmospheric and oceanic initial conditions) to better characterize the forced model's climate change projections, even for extreme forcing perturbations as is the case here.

Contrasted precipitation and circulation forced-responses arise depending on the strength of the AMOC in the preindustrial climate state, used as initial states. When the AMOC is weaker, the slowdown of the Walker circulation in response to increased CO_2 is amplified (compared to when the AMOC is stronger), which substantially influences the amplitude of rainfall changes over Indonesia, southeast Asia and the equatorial Pacific ocean. The direct CO_2-forced effect alone on circulation changes explains the overall sensitivity of precipitation and circulation forced-changes to AMOC states. A mechanism is proposed to explain how the direct weakening of the tropical circulation in response to CO_2 depends on AMOC-related background climate states. We show that:

1. Global energetic constraints on precipitation and water vapor explain the impact of different AMOC states on the mean tropical circulation in the control climate. When the AMOC is weak, a strengthening of the tropical overturning circulation (Hadley and Walker circulations) is obtained consistently with a significant decrease in global mean surface temperature.
2. The direct weakening of the circulation in response to increased CO_2 results from the dependence of the CO_2 radiative forcing on the spatial distribution of clouds and water vapor [*Merlis*, 2015]. Therefore, the stronger overturning circulation (when AMOC is weaker), which enhances the cloud and water vapor contrasts between convective and subsidence areas and thus the spatial heterogeneity of the CO_2 forcing, leads to a stronger direct weakening of the circulation.

Our interpretation provides an example of a new mechanism by which the response of tropical precipitation to CO_2 forcing depends on the background climate state. We call it the "strong-gets-weaker" mechanism, as it essentially operates through the circulation changes: the stronger the circulation in the control climate state, the weaker it gets in response to CO_2 forcing, enhancing the amplitude of rainfall changes at the regional scales. Although

the example given here explains the AMOC influence on Walker circulation forced changes, this mechanism might also provide the backdrop for any factor that influences the intensity of the mean tropical circulation in the control climate state. A point that should motivate further investigation for understanding the inter-model spread in CO_2-forced circulation changes.

These insights are based on the analysis of abrupt doubling CO_2 experiments; the question arises as to how relevant they are to interpret the AMOC influence on the climate response to gradually increasing CO_2 concentration. We analyzed twin ensemble transient climate change simulations using the exact same initial conditions, in which CO_2 increases at 2% per year until doubling the initial CO_2 concentration. We found very similar ensemble-mean sensitivities of precipitation and circulation forced-changes to AMOC states (Supplementary Fig. S7 – S14). Moreover, strong differences between respective members (from abrupt and transient CO_2 forcing experiments) are noticeable, despite the fact that they have the exact same initial conditions. This confirms the robustness of our results, which emphasize the very important role of the background climate state for the projected tropical and circulation changes, at least in the CNRM-CM5 model.

Acknowledgments

This work is supported by the French National Research Agency (ANR) project MORDICUS (ANR-13-SENV-0002-01). Primary data and scripts used in the analysis and other supplementary information are archived at `ftp://ftp.cerfacs.fr/pub/globc/exchanges/cassou/Data4Papers/GRL_Vial_etal_2018/`. We acknowledge the World Climate Research Programme's Working Group on Coupled Modelling, which is responsible for CMIP, and we thank the climate modeling groups (listed in Table S1 of this paper) for producing and making available their model output on the CEDA portal (http://browse.ceda.ac.uk). Additionally, we are grateful to the two reviewers for their helpful comments.

References

Bony, S., G. Bellon, D. Klocke, S. Sherwood, S. Fermepin, and S. Denvil (2013), Robust direct effect of carbon dioxide on tropical circulation and regional precipitation, *Nature Geoscience*, *6*(6), 447–451.

Buckley, M. W., and J. Marshall (2016), Observations, inferences, and mechanisms of the Atlantic Meridional Overturning Circulation: A review, *Reviews of Geophysics*, *54*(1), 5–63.

Cassou, C., Y. Kushnir, E. Hawkins, A. Pirani, F. Kucharski, S. Kang, and N. Caltabiano (2018), Decadal climate variability and predictability: challenges and opportunities, *Bulletin of the American Meteorological Society*, *99*(3), 479–490.

Chadwick, R., I. Boutle, and G. Martin (2013), Spatial patterns of precipitation change in CMIP5: Why the rich do not get richer in the tropics, *Journal of Climate*, *26*(11), 3803–3822.

Chou, C., and J. D. Neelin (2004), Mechanisms of global warming impacts on regional tropical precipitation, *Journal of climate*, *17*(13), 2688–2701.

Chou, C., J. D. Neelin, C.-A. Chen, and J.-Y. Tu (2009), Evaluating the "rich-get-richer" mechanism in tropical precipitation change under global warming, *Journal of Climate*, *22*(8), 1982–2005.

Collins, W., V. Ramaswamy, M. Schwarzkopf, Y. Sun, R. Portmann, Q. Fu, S. Casanova, J.-L. Dufresne, D. Fillmore, P. Forster, et al. (2006), Radiative forcing by well-mixed greenhouse gases: Estimates from climate models in the Intergovernmental Panel on Climate Change (IPCC) Fourth Assessment Report (AR4), *Journal of Geophysical Research: Atmospheres*, *111*(D14).

De Carvalho, L. M. V. (2016), *The monsoons and climate change: observations and modeling. In: de Carvalho L., Jones C. (eds) The Monsoons and Climate Change.*, 1–6 pp., Springer Climate, Switzerland.

Deser, C., A. Phillips, V. Bourdette, and H. Teng (2012), Uncertainty in climate change projections: the role of internal variability, *Climate Dynamics*, *38*(3-4), 527–546.

Hawkins, E., and R. Sutton (2011), The potential to narrow uncertainty in projections of regional precipitation change, *Climate Dynamics*, *37*(1-2), 407–418.

Hawkins, E., R. S. Smith, J. M. Gregory, and D. A. Stainforth (2016), Irreducible uncertainty in near-term climate projections, *Climate Dynamics*, *46*(11-12), 3807–3819.

Held, I. M., and B. J. Soden (2006), Robust responses of the hydrological cycle to global warming, *Journal of Climate*, *19*(21), 5686–5699.

Huang, Y., X. Tan, and Y. Xia (2016), Inhomogeneous radiative forcing of homogeneous greenhouse gases, *Journal of Geophysical Research: Atmospheres*, *121*(6), 2780–2789.

Huang, Y., Y. Xia, and X. Tan (2017), On the pattern of CO2 radiative forcing and poleward energy transport, *Journal of Geophysical Research: Atmospheres*.

Kang, S., C. Deser, and L. M. Polvani (2013), Uncertainty in climate change projections of the Hadley circulation, *Journal of Climate*, *26*, 7541–7554.

L'hévéder, B., F. Codron, and M. Ghil (2015), Impact of anomalous northward oceanic heat transport on global climate in a slab ocean setting, *Journal of Climate*, *28*(7), 2650–2664.

Long, S.-M., S.-P. Xie, and W. Liu (2016), Uncertainty in tropical rainfall projections: atmospheric circulation effect and the ocean coupling, *Journal of Climate*, *29*(7), 2671–2687.

Ma, J., and S.-P. Xie (2013), Regional patterns of sea surface temperature change: A source of uncertainty in future projections of precipitation and atmospheric circulation, *Journal of Climate*, *26*(8), 2482–2501.

Ménégoz, M., C. Cassou, D. Swingedouw, Y. Ruprich-Robert, P.-A. Bretonnière, and F. Doblas-Reyes (2017), Role of the Atlantic Multidecadal Variability in modulating the climate response to a Pinatubo-like volcanic eruption, *Climate Dynamics*, pp. 1–21, doi:10.1007/s00382-017-3986-1.

Merlis, T. M. (2015), Direct weakening of tropical circulations from masked CO_2 radiative forcing, *Proceedings of the National Academy of Sciences*, *112*(43), 13,167–13,171.

Mitchell, J. F., C. Wilson, and W. Cunnington (1987), On CO2 climate sensitivity and model dependence of results, *Quarterly Journal of the Royal Meteorological Society*, *113*(475), 293–322.

Neelin, J. D., and I. M. Held (1987), Modeling tropical convergence based on the moist static energy budget, *Monthly Weather Review*, *115*(1), 3–12.

Oueslati, B., S. Bony, C. Risi, and J.-L. Dufresne (2016), Interpreting the inter-model spread in regional precipitation projections in the tropics: role of surface evaporation and cloud radiative effects, *Climate dynamics*, *47*(9-10), 2801–2815.

Ruprich-Robert, Y., and C. Cassou (2015), Combined influences of seasonal east atlantic pattern and north atlantic oscillation to excite atlantic multidecadal variability in a climate model, *Climate Dynamics*, *44*(1-2), 229–253.

Seager, R., N. Naik, and G. A. Vecchi (2010), Thermodynamic and dynamic mechanisms for large-scale changes in the hydrological cycle in response to global warming, *Journal of Climate*, *23*(17), 4651–4668.

Selten, F. M., G. W. Branstator, H. A. Dijkstra, and M. Kliphuis (2004), Tropical origins for recent and future Northern Hemisphere climate change, *Geophysical Research Letters*, *31*(21), doi:10.1029/2004GL020739.

Taylor, K. E., R. J. Stouffer, and G. A. Meehl (2012), An overview of CMIP5 and the experiment design, *Bulletin of the American Meteorological Society*, *93*(4), 485–498.

Trenberth, K. E., and D. P. Stepaniak (2004), The flow of energy through the Earth's climate system, *Quarterly Journal of the Royal Meteorological Society*, *130*(603), 2677–2701.

Vecchi, G. A., and B. J. Soden (2007), Global warming and the weakening of the tropical circulation, *Journal of Climate*, *20*(17), 4316–4340.

Voldoire, A., E. Sanchez-Gomez, D. S. y Mélia, B. Decharme, C. Cassou, S. Sénési, S. Valcke, I. Beau, A. Alias, M. Chevallier, et al. (2013), The CNRM-CM5.1 global climate model: description and basic evaluation, *Climate Dynamics*, *40*(9-10), 2091–2121.

Xia, Y., and Y. Huang (2017), Differential Radiative Heating Drives Tropical Atmospheric Circulation Weakening, *Geophysical Research Letters*, *44*(20).

Xie, S.-P., C. Deser, G. A. Vecchi, J. Ma, H. Teng, and A. T. Wittenberg (2010), Global warming pattern formation: Sea surface temperature and rainfall, *Journal of Climate*, *23*(4), 966–986.

Xie, S.-P., C. Deser, G. A. Vecchi, M. Collins, T. L. Delworth, A. Hall, E. Hawkins, N. C. Johnson, C. Cassou, A. Giannini, and M. Watanabe (2015), Towards predictive understanding of regional climate change, *Nature Climate Change*, doi:10.1038/NCLIMATE2689.

Supporting Information for "Influence of the Atlantic meridional overturning circulation on the tropical climate response to CO_2 forcing"

Jessica Vial,[12] Christophe Cassou,[3] Francis Codron,[1] Sandrine Bony[4] and Yohan Ruprich-Robert[5]

Corresponding author: Jessica Vial, Max Planck Institute for Meteorology, Hamburg, Germany (jessica.vial@mpimet.mpg.de)

[1]LOCEAN/IPSL, Sorbonne Université, CNRS, Université Pierre et Marie Curie, France

[2]Max Planck Institute for Meteorology, Hamburg, Germany

[3]Université de Toulouse, CECI, CNRS-Cerfacs, France

[4]LMD/IPSL, Sorbonne Université, CNRS, Université Pierre et Marie Curie, France

[5]Barcelona Supercomputing Center, Barcelona, Spain

Contents of this file

Text S1. Origin of AMOC-related differences in tropical precipitation changes.

The impact of different AMOC-related background states on the 30-year mean CO_2-forced changes in tropical precipitation is here analysed using the monthly-mean vertically integrated water budget equation [e.g., *Chou et al.*, 2009; *Seager et al.*, 2010; *Bony et al.*, 2013; *Long et al.*, 2016] :

$$\Delta P = \Delta E - \Delta \left[\omega \Gamma_q\right] - \Delta \left[\vec{V}.\vec{\nabla} q\right] + res \tag{1}$$

where P is the surface precipitation (mm d^{-1}), E the surface evaporation (mm d^{-1}), ω the vertical pressure velocity profile (Pa s^{-1}), V the horizontal wind profile (m s^{-1}), q the specific humidity profile ($\times L_v$, in J kg^{-1}), Γ_q its vertical gradient (J kg^{-1} Pa^{-1}) and ∇q its horizontal gradient (J kg^{-1} m^{-1}) and res is the residual term owing to sub-monthly transient eddy convergence. Square brackets refer to mass-weighted vertical integrals and Δ refers to 30-year CO_2-forced changes.

Figure S2 shows that the change in vertical moisture advection ($\Delta \left[\omega \Gamma_q\right]$ in Fig. S2d) is clearly the dominant source of AMOC-related differences in the tropical precipitation change, with negligible contributions from the other three terms. We further decompose the vertical advection term into a thermodynamic and a dynamic component to diagnose the relative contributions of moisture and circulation changes, respectively [e.g., *Seager et al.*, 2010; *Long et al.*, 2016] : $\Delta \left[\omega \Gamma_q\right] = \Delta P_{ther} + \Delta P_{dyn}$, where $\Delta P_{ther} = \left[\omega \Delta \Gamma_q\right]$ and $\Delta P_{dyn} = \left[\Gamma_q \Delta \omega\right]$. Figure S3 shows that all of the difference in tropical precipitation changes between the cold and warm ensembles is due to ΔP_{dyn} (Fig. S3b).

The separate influence of the AMOC state on the preindustrial moisture profile and on the

forced changes in the mean circulation is then assessed by expressing the dynamical component as the product of surface specific humidity in unperturbed (P-ensemble) climate simulations (q_{sfc}) and CO_2-forced change in mid-tropospheric vertical motion ($\Delta\omega_{500}$) : $\Delta P_{dyn} \simeq -\frac{1}{g} q_{sfc} \Delta\omega_{500}$. This has been shown to be a good approximation for the Tropics [*Held and Soden*, 2006; *Huang et al.*, 2013; *Huang*, 2014; *Long et al.*, 2016; *Wills and Schneider*, 2016]; here, the correlation across all experiments between ΔP_{dyn} and $-\frac{1}{g} q_{sfc} \Delta\omega_{500}$ in the two main areas where the difference between the cold and warm ensembles is strong (the Niño 3 and Niño 4 regions) is close to unity.

Figures S4 shows that $\Delta\omega_{500}$ accounts for most of the difference in the tropical rainfall changes between the cold and warm ensembles (Figures S4b) and of the variance in ΔP across the warm and cold ensembles (Fig. S4d and S4f). Therefore, it is clear that the influence of the AMOC on the change in tropical precipitation operates essentially through the modulation of the mean circulation changes, and especially of its zonally asymmetric component (the Walker circulation, Fig. S5c).

Text S2. Robustness of the relationship between the low-frequency variations of the AMOC and of the tropical atmospheric circulation

In the CNRM-CM5 multi-member ensembles that we use for this study, we compare two extreme states of the AMOC that are associated with pronounced and persistent negative/positive phases of the AMV, which in turn affect the climate at the global scale. However, the spatio-temporal properties of the simulated AMOC and AMV, the relationship between

them and their influence on climate at the larger scale can vary substantially between models [e.g., *Zhang and Wang*, 2013; *Ba et al.*, 2014; *Qasmi et al.*, 2017; *Yan et al.*, 2018]. Moreover, in most models the persistence, amplitude and large-scale spatial coherence of the AMOC and AMV are underestimated with respect to observations [e.g., *Qasmi et al.*, 2017; *Yan et al.*, 2018] – keeping in mind the large uncertainties also in the observations due to sampling and the different existing methodologies for extracting externally forced variations [*Qasmi et al.*, 2017]. The CNRM-CM5 model is no exception to these systematic biases, although it lies above the multi-model mean for the persistence and amplitude of the AMV [*Qasmi et al.*, 2017, their Fig. 1 and Supplementary Fig. S6] and tends to have a stronger hemispheric-scale temperature response to AMOC fluctuations compared to other models [*Yan et al.*, 2018, their Fig. 3].

Given the large diversity in model behaviors, we here aim to provide some insights into the robustness of our findings across different coupled models, and especially regarding the relationship between the AMOC and the atmospheric tropical circulation in the control climate state (cf. Section 5.1), which is determining in the sensitivity of the CO_2-forced tropical climate response to the AMOC state in the CNRM-CM5 model. More specifically, here we address the question of whether or not the global energetic framework (described in Section 5.1) can robustly constrain the response of the atmospheric tropical overturning circulation to the AMOC/AMV state in the control climate. To do so, we perform a similar analysis as in Figure 3, but by compositing the tropically-averaged climate variables and atmospheric circulation indices with respect to positive/negative phases of the AMV across 28 coupled model simulations using the long piControl experiments of the CMIP5 archive (cf. Table S1).

Among those models, upon availability of the ocean meridional overturning circulation data, 8 were also retained to assess the relationship with respect to the AMOC phases. The AMV index is defined as the detrended, low-pass filtered annual North Atlantic SST anomalies averaged over 0°-60°N and 0°-80°W [e.g., *Qasmi et al.*, 2017], using a 30-year low-pass filter (instead of the more traditional 10-year filter) to be more comparable with the 30-year averaged periods used in our main analysis. The AMOC index is similarly defined as detrended, 30-year low-pass filtered annual anomalies, but from the maximum meridional stream function deeper than 500 m at 26°N [*Qasmi et al.*, 2017].

The results presented in Figure S6 clearly show that the relationship between the phase of the AMOC/AMV and the strength of the atmospheric tropical circulation (I) is robust across CMIP5 models and well explained by the global constraints on precipitation and water vapor (Fig. S6a – d). This is also true for the Walker circulation, which is strongly related to the multidecadal variations of the tropical mean overturning circulation (Fig. S6f). However, the AMOC/AMV-related variations in the Hadley circulation appear to be more model-dependent (Fig. S6a – e). One possible explanation could be related to different sensitivities of the Hadley/Walker circulations to the spatio-temporal properties of the simulated AMOC/AMV. For instance, *Delworth and Zeng* [2016] have recently shown that the hemispheric-scale climate response (including the ITCZ/Hadley circulation) to AMOC variations can be considerably stronger for longer time scales of the AMOC fluctuations ($>$ 50 years). Another reason could be due to the relative weight between tropical – extratropical teleconnections and local tropical feedbacks in a given model, which have opposite effects on the response of the ITCZ/Hadley circulation to extratropical forcing [*Kang et al.*, 2018]. The multi-model analysis presented here

should motivate further research to better understand the differences in the Hadley/Walker circulation responses to low-frequency AMOC/AMV fluctuations.

References

Ba, J., N. S. Keenlyside, M. Latif, W. Park, H. Ding, K. Lohmann, J. Mignot, M. Menary, O. H. Otterå, B. Wouters, et al. (2014), A multi-model comparison of Atlantic multidecadal variability, *Climate dynamics*, *43*(9-10), 2333–2348.

Bony, S., G. Bellon, D. Klocke, S. Sherwood, S. Fermepin, and S. Denvil (2013), Robust direct effect of carbon dioxide on tropical circulation and regional precipitation, *Nature Geoscience*, *6*(6), 447–451.

Chou, C., J. D. Neelin, C.-A. Chen, and J.-Y. Tu (2009), Evaluating the "rich-get-richer" mechanism in tropical precipitation change under global warming, *Journal of Climate*, *22*(8), 1982–2005.

Delworth, T. L., and F. Zeng (2016), The impact of the North Atlantic Oscillation on climate through its influence on the Atlantic meridional overturning circulation, *Journal of Climate*, *29*(3), 941–962.

Held, I. M., and B. J. Soden (2006), Robust responses of the hydrological cycle to global warming, *Journal of Climate*, *19*(21), 5686–5699.

Huang, P. (2014), Regional response of annual-mean tropical rainfall to global warming, *Atmospheric Science Letters*, *15*(2), 103–109.

Huang, P., S.-P. Xie, K. Hu, G. Huang, and R. Huang (2013), Patterns of the seasonal response of tropical rainfall to global warming, *Nature Geoscience*, *6*(5), 357–361.

Kang, S. M., Y. Shin, and S.-P. Xie (2018), Extratropical forcing and tropical rainfall distribution: energetics framework and ocean Ekman advection, *npj Climate and Atmospheric Science*, *1*(1), 2.

Long, S.-M., S.-P. Xie, and W. Liu (2016), Uncertainty in tropical rainfall projections: atmospheric circulation effect and the ocean coupling, *Journal of Climate*, *29*(7), 2671–2687.

Qasmi, S., C. Cassou, and J. Boé (2017), Teleconnection Between Atlantic Multidecadal Variability and European Temperature: Diversity and Evaluation of the Coupled Model Intercomparison Project Phase 5 Models, *Geophysical Research Letters*, *44*(21), 11–140.

Seager, R., N. Naik, and G. A. Vecchi (2010), Thermodynamic and dynamic mechanisms for large-scale changes in the hydrological cycle in response to global warming, *Journal of Climate*, *23*(17), 4651–4668.

Wills, R. C., and T. Schneider (2016), How stationary eddies shape changes in the hydrological cycle: Zonally asymmetric experiments in an idealized GCM, *Journal of Climate*, *29*(9), 3161–3179.

Yan, X., R. Zhang, and T. R. Knutson (2018), Underestimated AMOC variability and implications for AMV and predictability in CMIP models, *Geophysical Research Letters*, *45*(9), 4319–4328.

Zhang, L., and C. Wang (2013), Multidecadal North Atlantic sea surface temperature and Atlantic meridional overturning circulation variability in CMIP5 historical simulations, *Journal of Geophysical Research: Oceans*, *118*(10), 5772–5791.

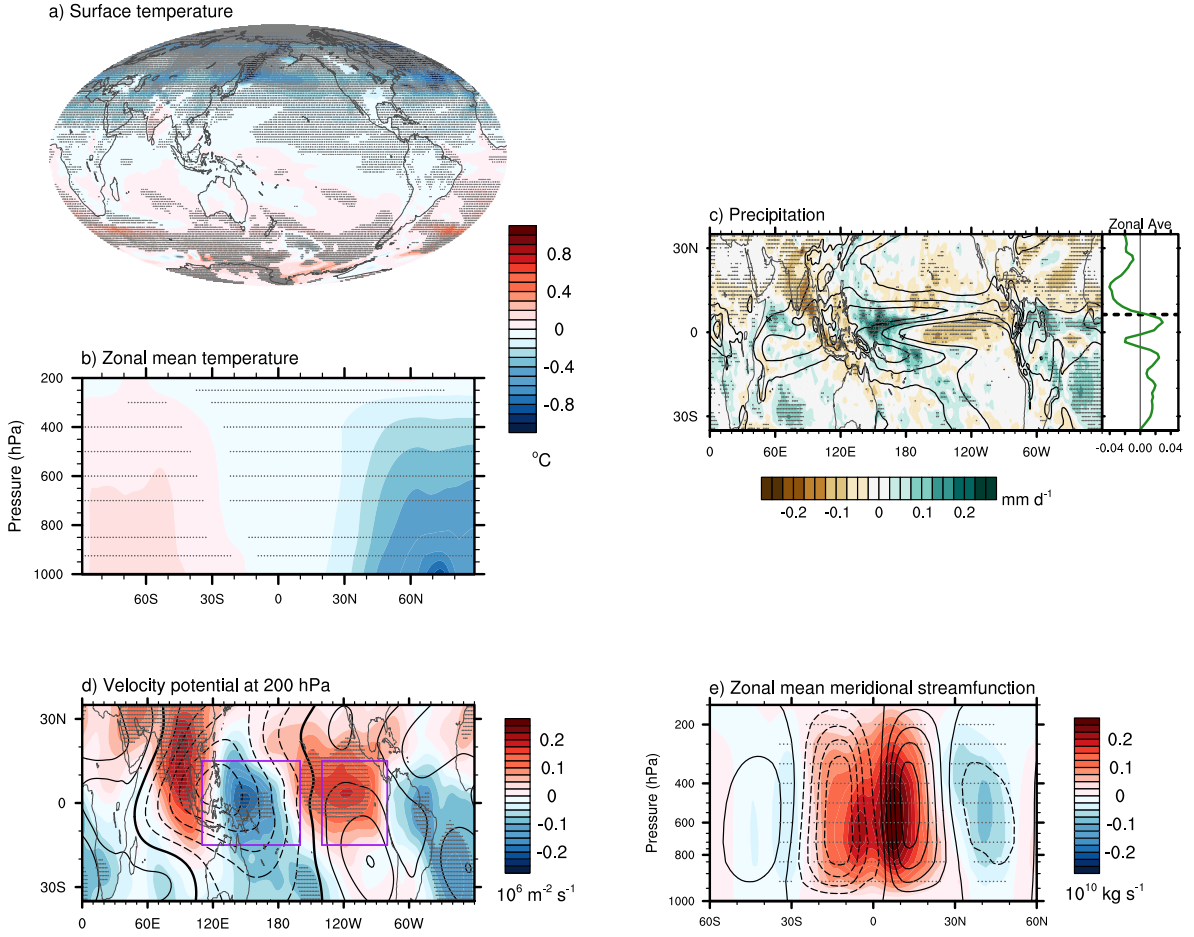

Figure S1: AMOC-related difference between the cold and warm ensembles for (a) surface temperature, (b) zonal mean atmospheric temperature, (c) precipitation, with zonal mean values on the right panel, (d) velocity potential at 200 hPa and (e) zonal mean meridional streamfunction. Hatching indicates statistical significance (p=0.1). The contour lines in (c – e) represent the precipitation, velocity potential and meridional streamfunction climatologies from the 850-yr piControl model run. The dashed line in the zonal mean precipitation plot (c) is the climatological position of the ITCZ. The purple boxes indicate areas used to compute the Walker circulation index.

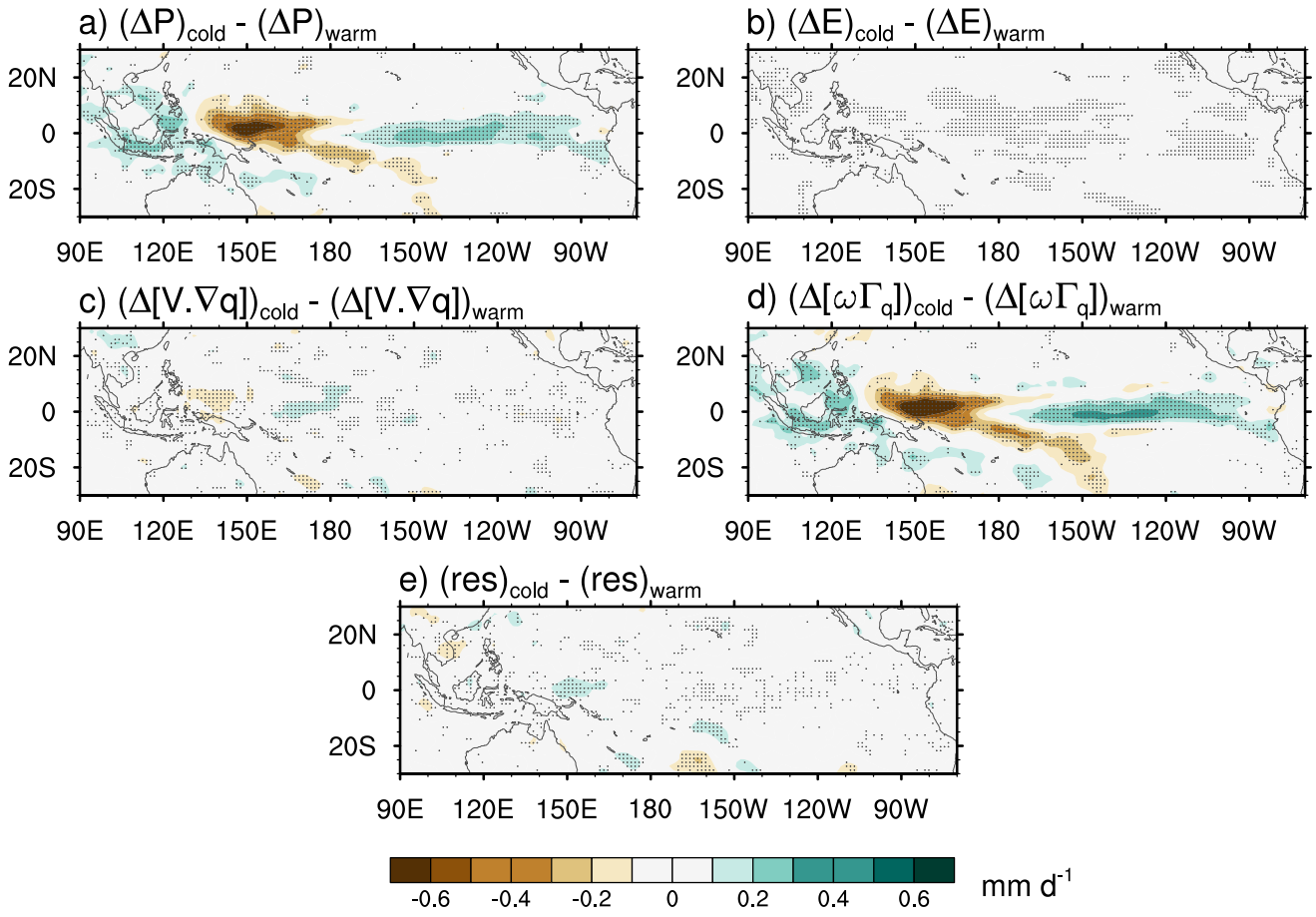

Figure S2: AMOC-related difference between the cold and warm ensembles for the forced changes in (a) surface precipitation ΔP, (b) surface evaporation ΔE, (c) vertically-integrated horizontal moisture advection $\Delta\left[\vec{V}.\vec{\nabla}q\right]$ and (d) vertical moisture advection $\Delta\left[\omega\Gamma_q\right]$ and (e) residual term in Eq. 1. Hatching indicates statistical significance (p=0.1).

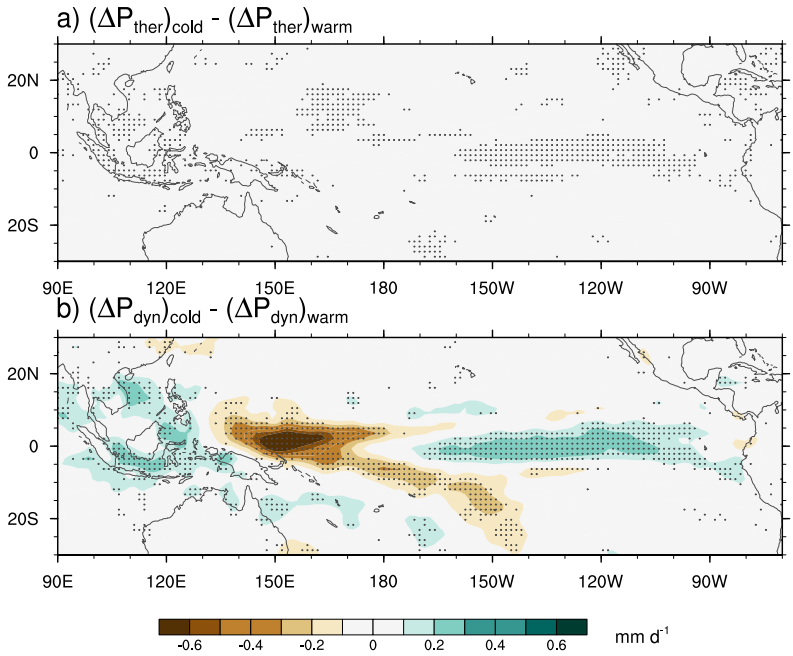

Figure S3: AMOC-related difference between the cold and warm ensembles for the (a) thermodynamic and (b) dynamic component of the forced change in precipitation. Hatching indicates statistical significance (p=0.1).

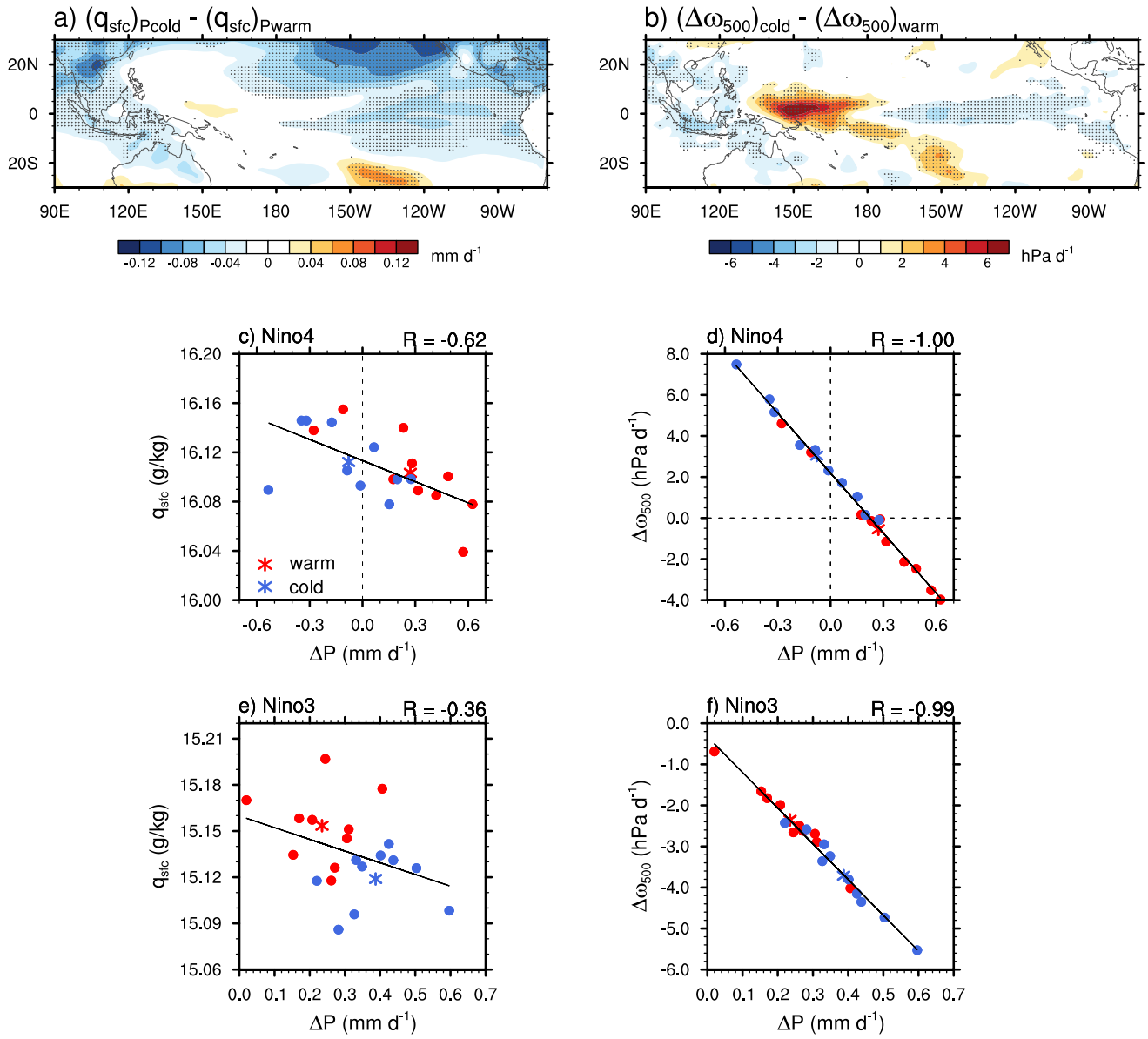

Figure S4: AMOC-related difference between the cold and warm ensembles for (a) surface specific humidity in P-ensemble simulations and (b) forced changes in mid-tropospheric circulation. Hatching indicates statistical significance (p=0.1). (c) Surface specific humidity in P-ensemble simulations and (d) forced changes in mid-tropospheric circulation as a function of the forced changes in precipitation over the Niño 4 region (5°S-5°N, 160°E-150°W). (e – f) same as (c – d) but for the Niño 3 region (5°S-5°N, 90°-150°W). Each individual member is represented by a filled circle and the ensemble means by asterisks.

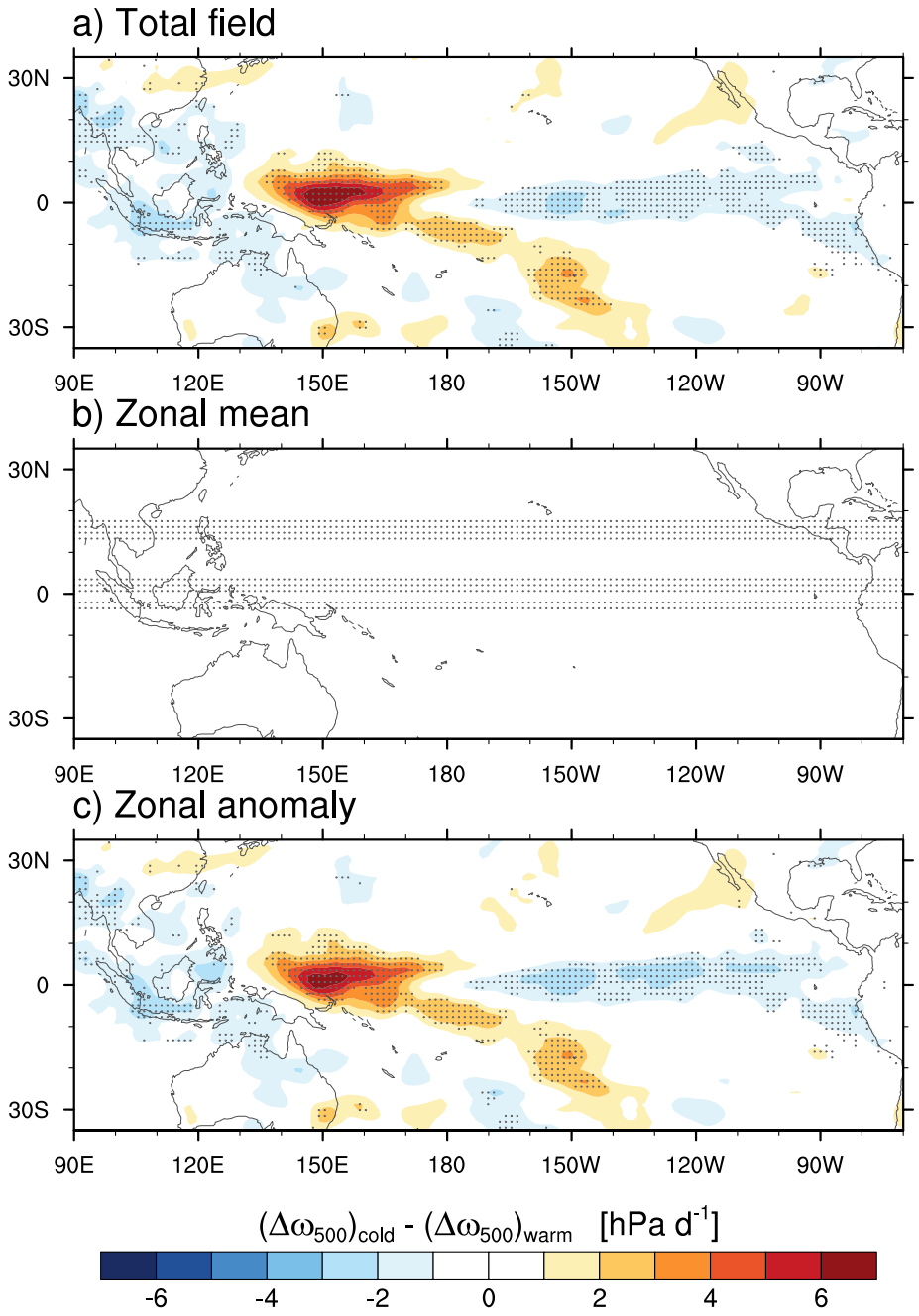

Figure S5: AMOC-related difference between the cold and warm ensembles for (a) the forced change in mid-tropospheric circulation, (b) its zonal mean component and (c) zonal anomaly component. Hatching indicates statistical significance (p=0.1).

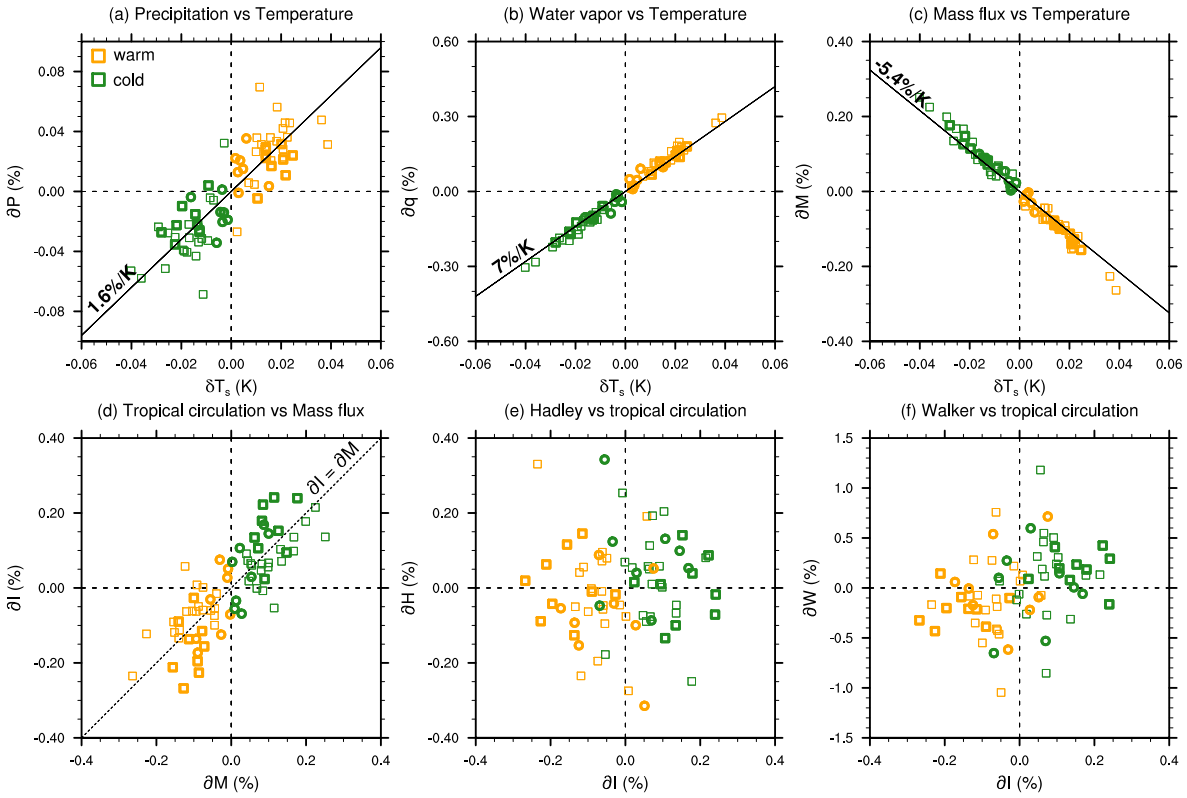

Figure S6: Same as Figure 3 but for composites with respect to warm/cold AMV phases in 28 climate model piControl simulations (squares) and strong/weak AMOC phases for a subset of 8 models (circles). For these 8 models, the AMOC/AMV points are shown with thicker markers. The color code is the same as in Figure 3: warm/strong (cold/weak) phases are shown by orange (green) markers.

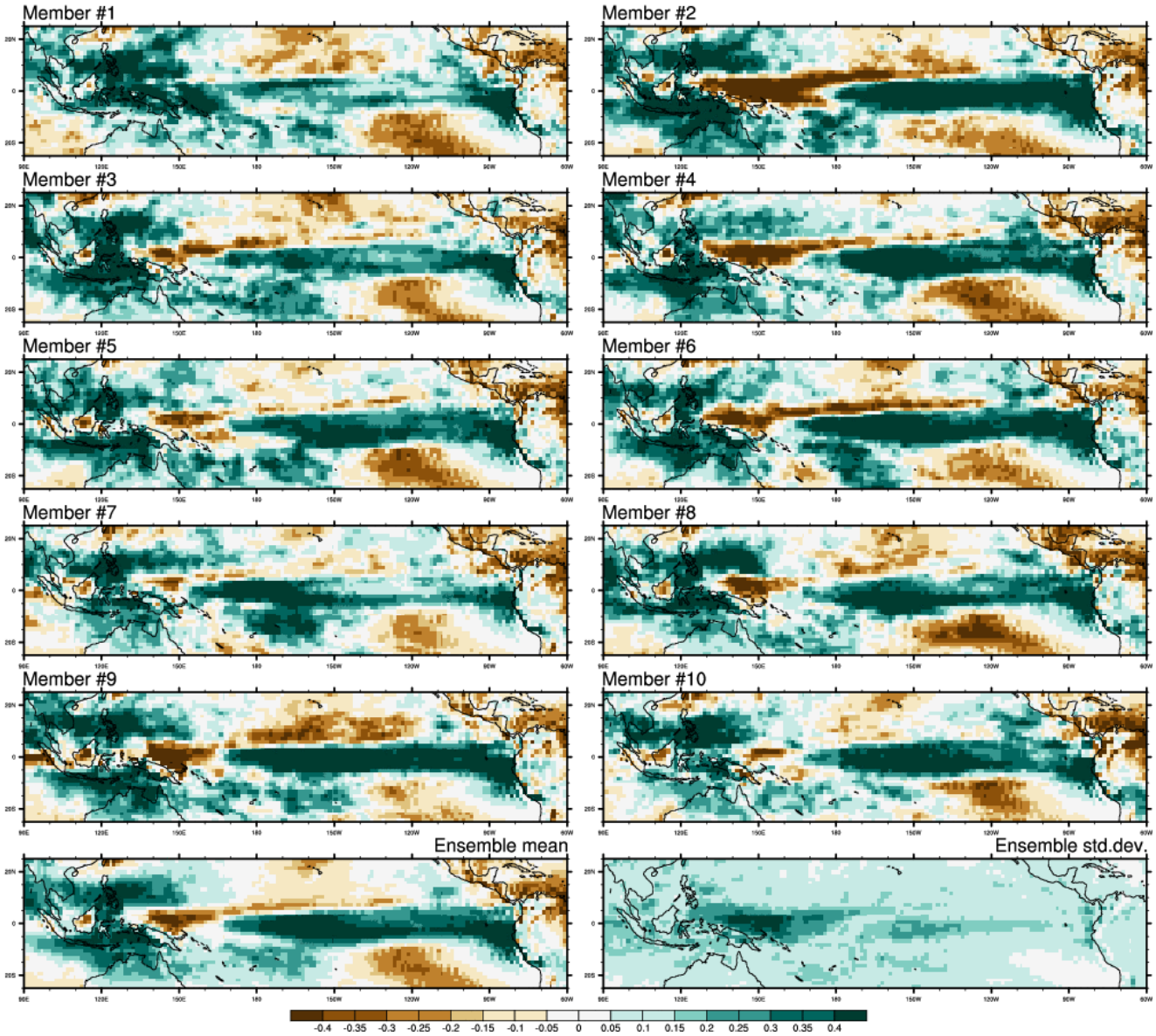

Figure S7: 30-year abrupt CO_2-forced change in precipitation (in mm d^{-1}) over tropical Pacific for all individual members of the cold ensemble. The panels on the last row show the ensemble mean (left) and ensemble standard deviation (right).

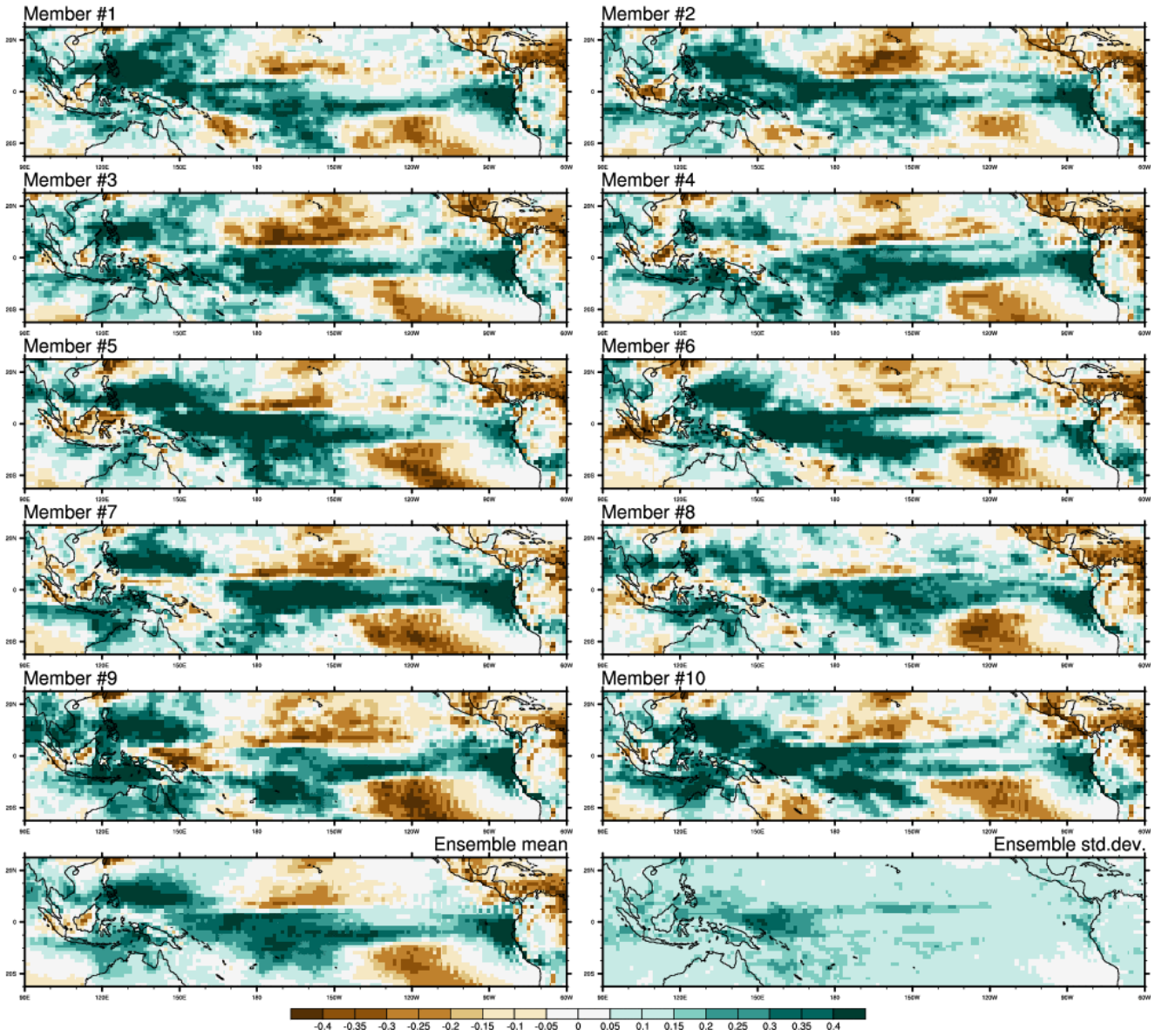

Figure S8: Same as Figure S7 but for the warm ensemble: abrupt CO_2-forced change in precipitation in the warm ensemble.

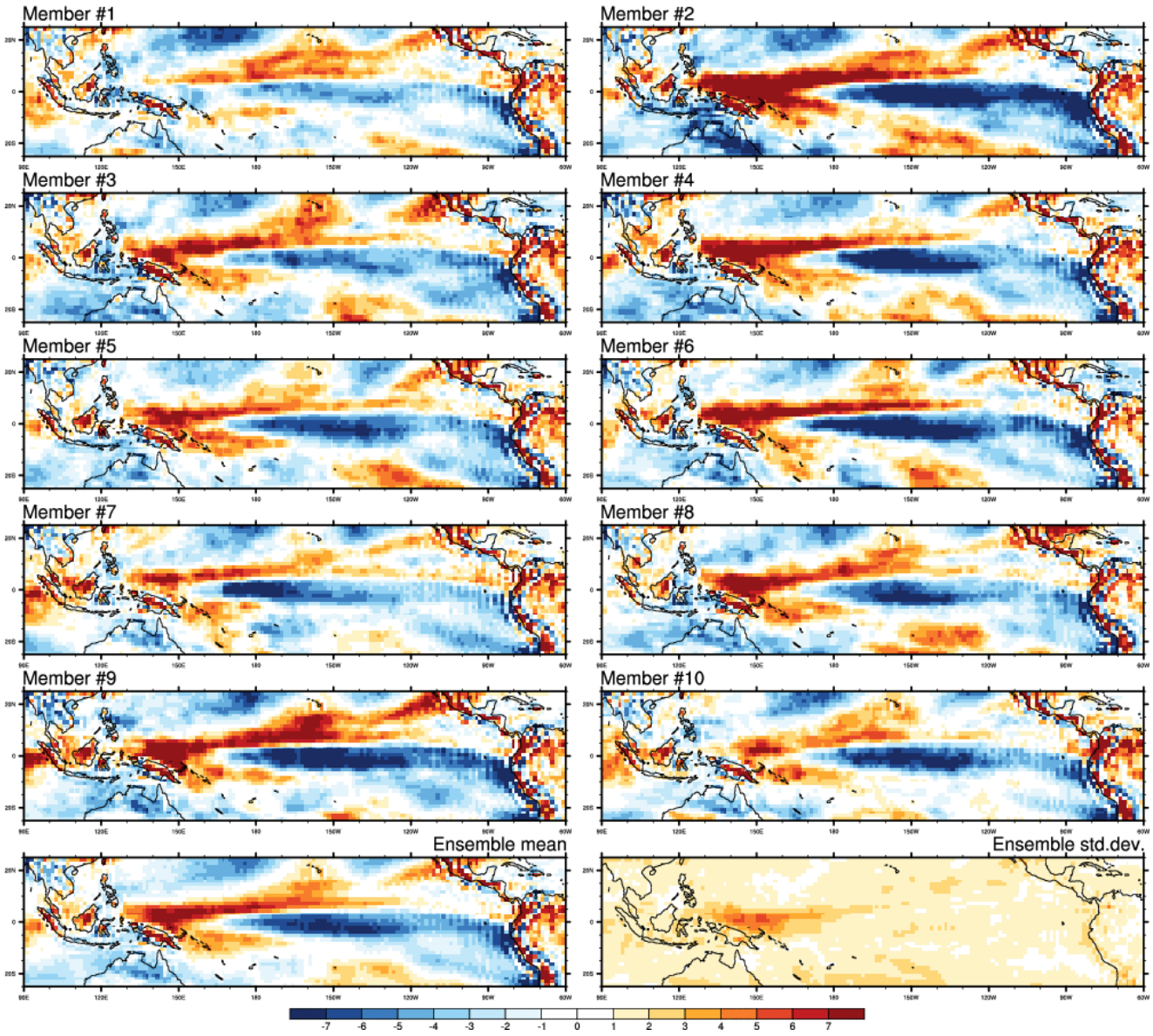

Figure S9: Same as Figure S7 but for abrupt CO_2-forced change in mid-tropospheric circulation (assessed with ω_{500}, in hPa d^{-1}) in the cold ensemble.

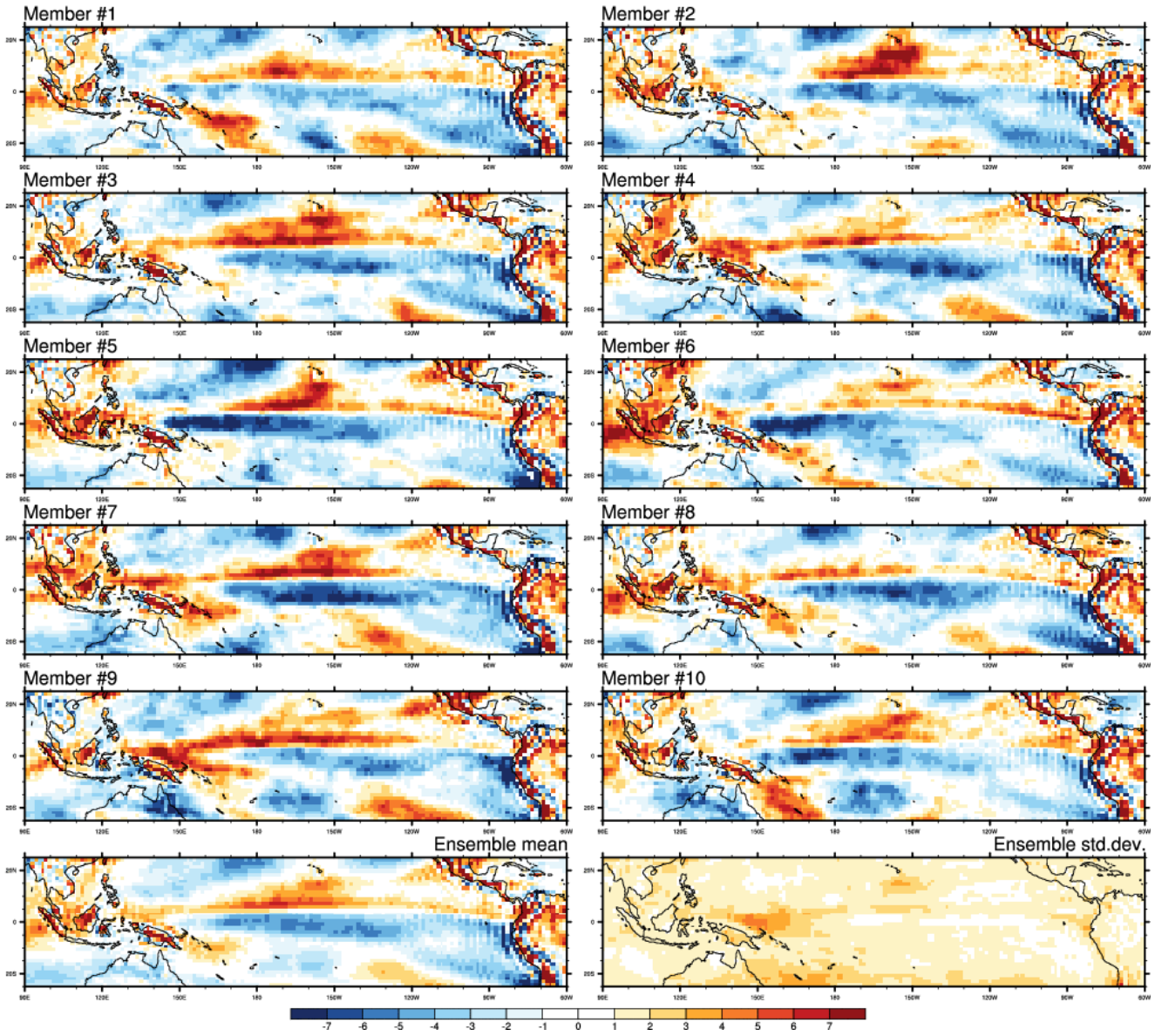

Figure S10: Same as Figure S8 but for the warm ensemble : abrupt CO_2-forced change in ω_{500} in the warm ensemble.

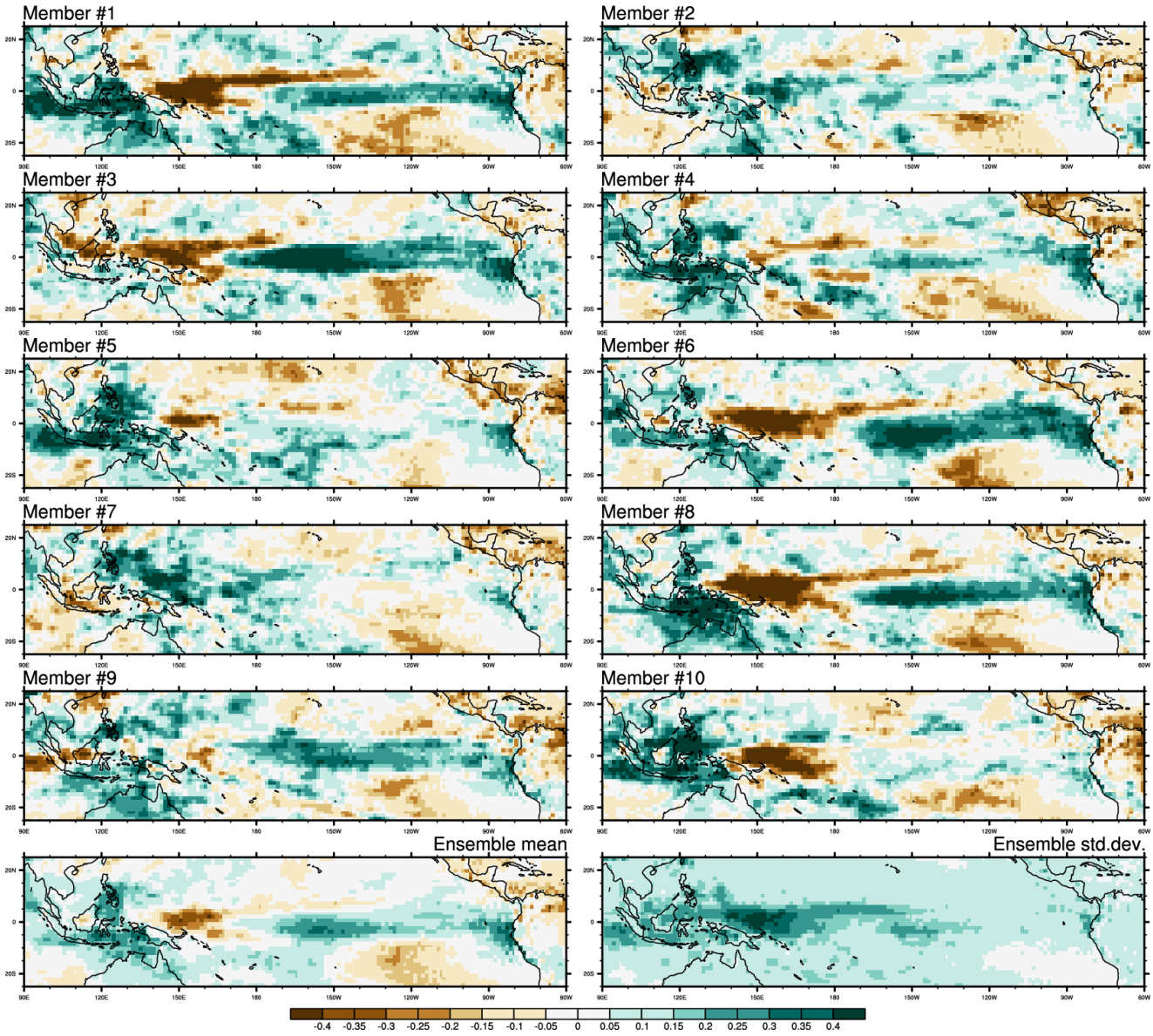

Figure S11: Same as Figure S7 but for transient CO_2-forced experiments: change in precipitation in the cold ensemble

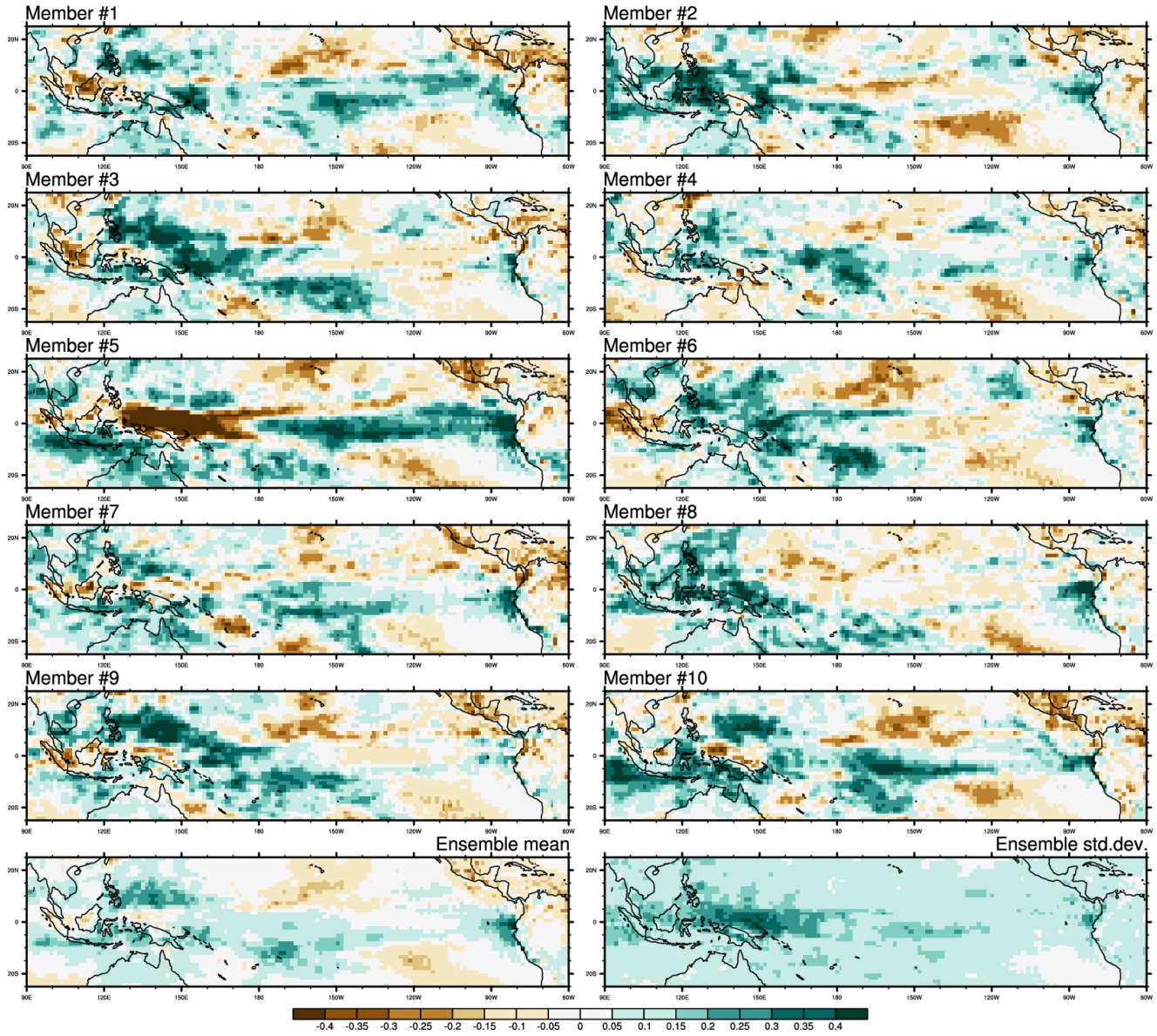

Figure S12: Same as Figure S8 but for transient CO_2-forced experiments: change in precipitation in the warm ensemble

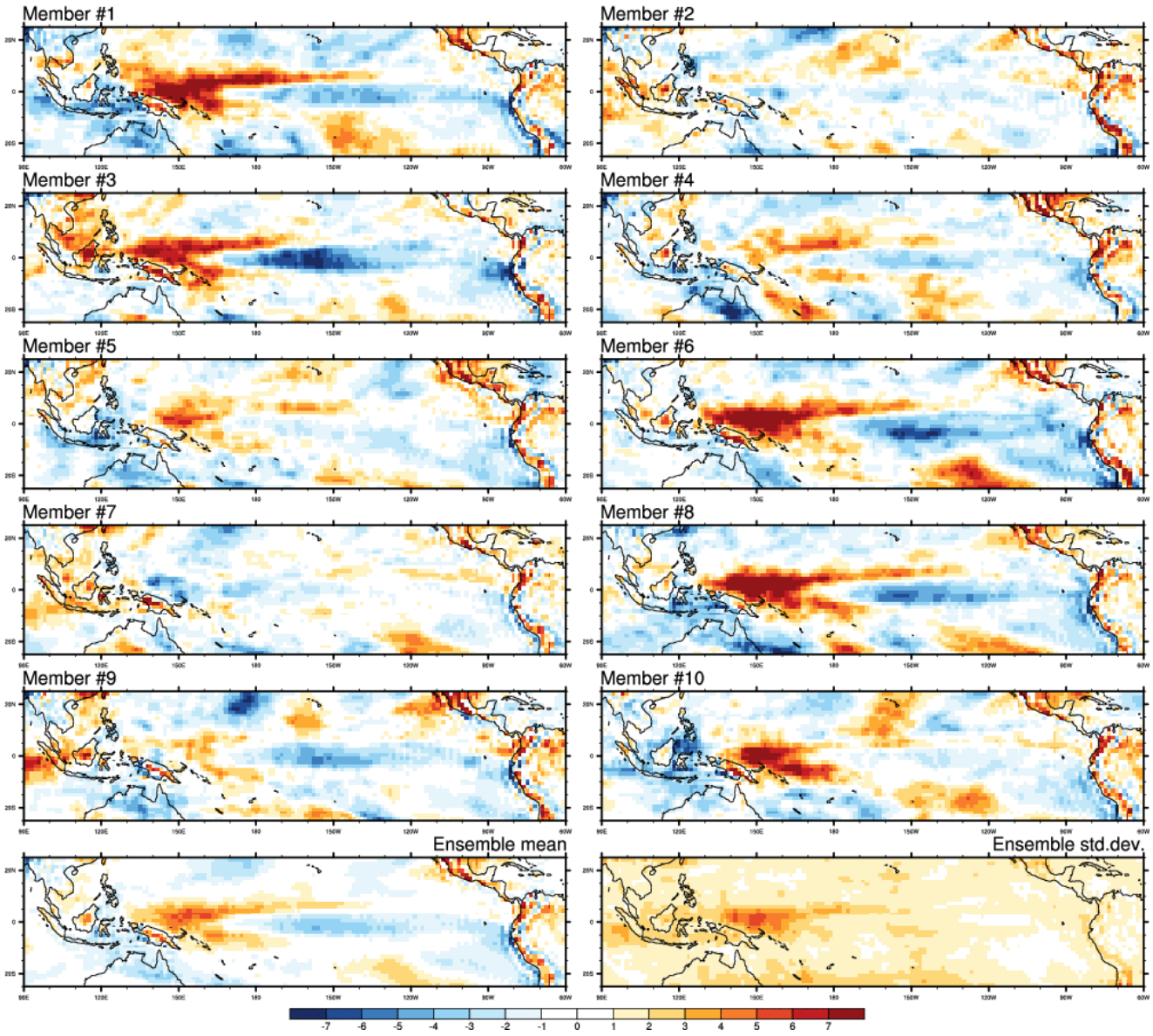

Figure S13: Same as Figure S9 but for transient CO_2-forced experiments: change in ω_{500} in the cold ensemble

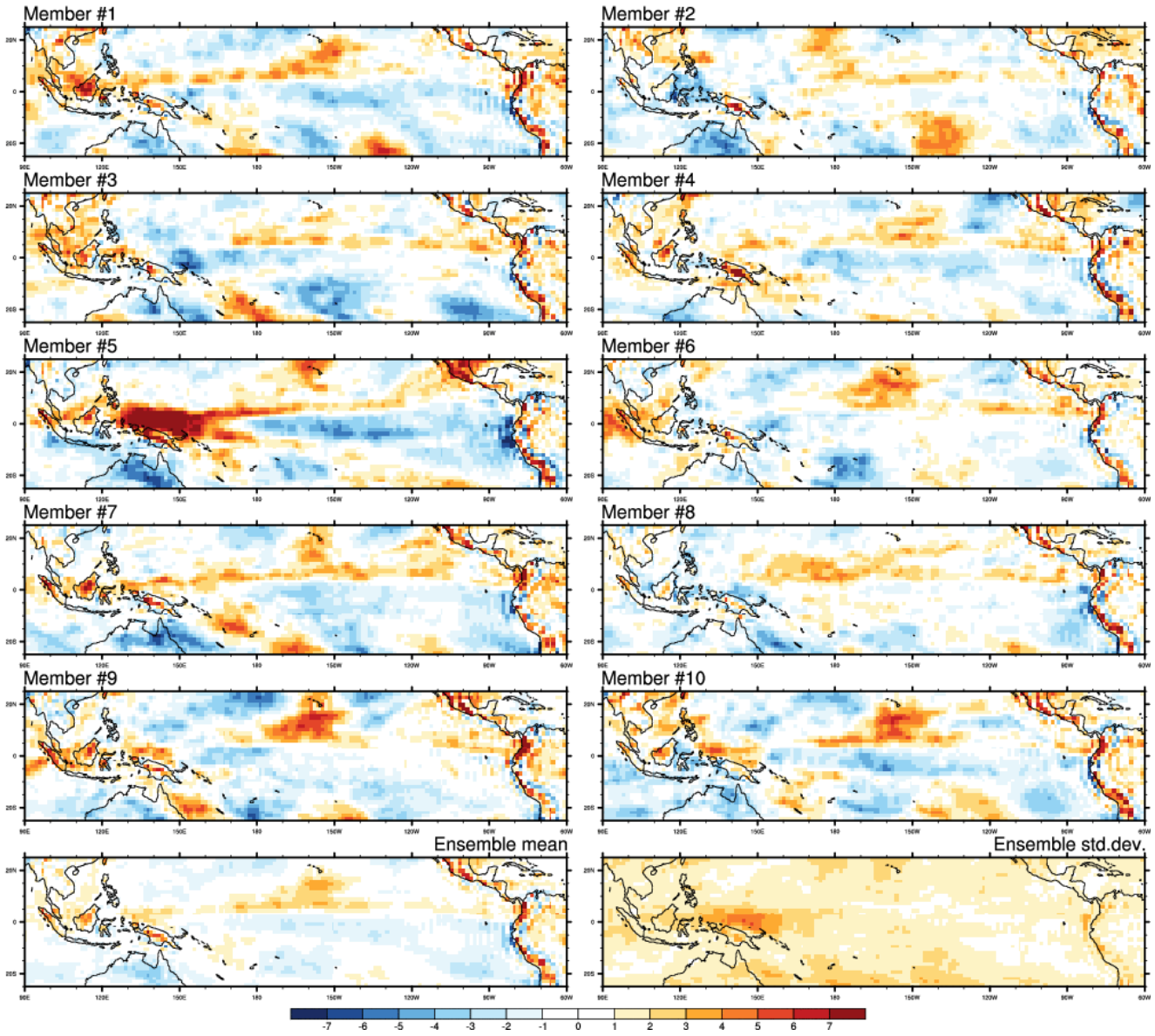

Figure S14: Same as Figure S10 but for transient CO_2-forced experiments: change in ω_{500} in the warm ensemble

Table S1: List of the CMIP5 coupled models used to produce the AMOC/AMV compositing analysis in Figure S6, together with the respective length of their picontrol simulations (in years). The 8 models retained for the AMOC analysis are in bold.

Model acronyms	Number of years
CESM1-CAM5	319
GFDL-ESM2M	500
GFDL-ESM2G	500
GFDL-CM3	500
NorESM1-M	501
CCSM4	501
GISS-E2-R	850
MRI-CGCM3	500
MPI-ESM-P	1156
MPI-ESM-MR	1000
MPI-ESM-LR	1000
MIROC-ESM	630
MIROC5	670
FGOALS-s2	501
FGOALS-g2	700
IPSL-CM5B-LR	300
IPSL-CM5A-MR	300
IPSL-CM5A-LR	1000
inmcm4	500
CSIRO-Mk3-6-0	500
ACCESS1-3	500
ACCESS1-0	500
CNRM-CM5	850
CMCC-CM	330
CanESM2	996
BNU-ESM	559
bcc-csm1-1	500
bcc-csm1-1-m	400